ORNL
MASTER COPY

DEC 2 1988

NOTICE This document contains information of a preliminary nature. It is subject to revision or correction and therefore does not represent a final report.

ORNL/ACP/LTR-88/1

Contract Program: Advanced Controls (ACTO) Program

Subject Of Document: Investigation of Reactivity Feedback Effects and Design of an Inherent Reactor Power Controller for a Metal-Fueled Advanced Liquid Metal Reactor

Type of Document: Letter Report

Authors: Richard T. Wood
Thomas L. Wilson, Jr.

Date of Document: October, 1988

DOE/HQ Monitor: H. Alter, Division of Advanced Technology Development

[redacted]

[redacted]

Prepared by
Instrumentation and Controls Division
OAK RIDGE NATIONAL LABORATORY
Oak Ridge, Tennessee 37831
operated by
MARTIN MARIETTA ENERGY SYSTEMS, INC.
for the
U. S. DEPARTMENT OF ENERGY
under Contract No. DE-AC05-84OR21400

ABSTRACT

Inherent power control for current metal-fueled advanced liquid metal reactor designs uses reactivity thermal feedback effects to control the power generated in the core instead of directly regulating reactor power through control rod action. This report presents the study of the inherent feedback characteristics of a metal fueled liquid metal reactor and the design of a load following controller that takes advantage of the inherent neutron power behavior for reactor power control during normal operation. Using the MMS-SAFR computer model, the dynamic response of the metal-fueled Sodium Advanced Fast Reactor has been evaluated as a representative liquid metal reactor design. The frequency response of each reactivity feedback effect is presented with an evaluation of the dynamic behavior of the reactivity contributions for core heat removal manipulations. The limitations on the open-loop reactivity response to changes in core temperatures caused by altering heat removal are discussed based on the insight gained from frequency domain observations and a sample flow reduction transient simulated with no control action on the system. From this investigation, it is seen that the feedback characteristics are sufficiently fast and strong that inherent reactor power control is feasible. However, control of selected coolant temperatures is desirable to facilitate tighter control over the inherent neutron power behavior. Candidate control parameters, such as primary, intermediate and steam generator flows, are investigated to select the most suitable control relationships. Based on classical frequency domain techniques, a proportional-integral control system design utilizing inherent reactor power control is described. The results of the frequency response analysis are used to select the input to output relationships for the control system and to set preliminary gains. Root locus design techniques are used to tune gains for satisfactory stability and transient response. The control strategy chosen actively controls steam generator power and reactor power control is passive, with the inherent reactivity feedback response maintaining a balance between power production in the core and power removal in the balance of plant. The inherent reactor power control scheme implemented on the MMS-SAFR model successfully followed a 10% step reduction in load demand within 35 seconds of the transient initiator, with the reactor following more slowly, while yielding only a 9°F temperature rise in the mixed average core outlet temperature during the event. This simulation shows the ability of a metal-fueled liquid metal reactor to use inherent reactivity effects for following electrical grid demand under normal operating conditions; however, because of loop delays, the speed of response for reactor power is limited in the control design to maintain stability.

SUMMARY

Inherent power control for current metal-fueled advanced liquid metal reactor designs proposes using reactivity thermal feedback effects to control the power generated in the core instead of directly regulating reactor power through control rod action. Essentially, inherent control of reactor power involves altering core heat removal, and thus reactor temperatures, to effect a power change rather than acting on heat production directly. This report presents the work performed at the Oak Ridge National Laboratory to study the reactor power control capabilities of the inherent reactivity feedback effects in a metal-fueled liquid metal reactor design. The purpose of this study is to evaluate the feasibility of power control based on inherent reactivity effects for a metal-fueled liquid metal reactor and to determine the extent to which normal load following requirements can be met by such control. Based on the results of this investigation, an inherent reactor power control strategy for normal operating events in the 40% to 100% power range has been devised and implemented in a computer simulation of a representative metal-fueled advanced liquid metal reactor. In this control scheme, the goal of balancing the heat generation and heat removal in the reactor system is achieved by altering the core temperatures through control action on the heat removal in the coolant loops and balance of plant rather than by direct control of heat production through control rod maneuvers.

The metal-fueled liquid metal reactor design studied is the Sodium Advanced Fast Reactor using the MMS-SAFR modular computer representation of the plant. MMS-SAFR, developed for use in the Advanced Controls program, is a full plant description of the SAFR design which simulates all the dynamic couplings between the primary and intermediate heat transport systems and the reactor kinetics. The modeling equations in MMS-SAFR are derived from the SASSYS analysis code, developed at the Argonne National Laboratory, by simplifying the formulation while maintaining the dynamic response characteristics. In this study, the linearized state space matrices are calculated from the nonlinear model and input to the Matrix_x controls analysis code to determine the frequency response of selected system parameters to chosen system inputs.

The frequency response of each reactivity feedback effect is presented with an evaluation of the dynamic behavior of the reactivity contributions for core heat removal manipulations. The behavior of the net reactivity was investigated along with the component reactivity effects to determine the physical processes that lead to inherent stability and, potentially, control. The limitations on the open-loop reactivity response to changes in core temperatures caused by altering heat removal are discussed based on the insight gained from frequency domain observations and

a sample flow reduction transient simulated with no control action on the system. From this investigation, it is seen that the feedback characteristics are sufficiently fast and strong that inherent reactor power control is feasible. The key to enabling inherent reactor power control is to perturb the appropriate process(es) to ensure that the inherent feedback response acts rapidly enough and without large swings in the system state to meet normal duty cycle demands. In addition, the long term response of the reactivity components, some of which are strongly affected by the inlet coolant temperature behavior, determines the degree to which steady state power can be changed as the overall reactivity approaches an equilibrium condition. By controlling coolant loop temperatures, through flow manuevers, the feedback response can be directed by a scheme to control reactor power without direct action on heat generation as the system inherently seeks to match power production with power removal.

The objective of the control design exercise performed in this study is to design a simple control system that gives acceptable load following performance over a plant power range of 40% to 100% while utilizing the inherent feedback behavior to control reactor power. The MMS-SAFR plant model is a multi-input, multi-output system. The strategy for this control design exercise is to use a system of classical, proportional-integral, feedback controllers. The MMS-SAFR inputs and outputs are broken into individual control loops, each with a single-input, single-output relationship. The frequency response plots are used to select the input to output relationships and to set the preliminary gains. The features of the frequency response plots, such as corner or break frequency and phase crossover frequency, give the needed insight to select good input to output relationships for control. The control system gains are then refined using the root locus method to enhance system stability while maintaining controller performance.

Candidate control parameters, such as primary loop, intermediate loop and steam generator flows, are investigated to select the most suitable mechanism for instigating the desired reactivity feedback response. The frequency domain controls analysis based on the response of various "observables" to change in selected "controllables" leads to the selection of feedwater flow as the control mechanism for actively matching steam generator power to load demand while steam flow and the two coolant loop flows are used to control steam pressure and selected coolant temperatures. This strategy provides for the inherent reactivity feedback effects to control reactor power in response to temperature changes resulting from action by the control system. Preliminary gains for these controllers are graphically chosen from the frequency response plots and are implemented in the model. Root locus design techniques are used to tune gains for satisfactory stability and transient response. The control strategy chosen actively controls steam generator power rather

than reactor power since maintaining an in-phase relationship between the turbine and electrical generator is key to load following. The reactor power control is passive, where the inherent reactivity feedback response maintains a balance between core power production and balance of plant power removal.

This study of inherent reactor power control shows that the delayed response of the reactor to steam generator load changes places a stability limit on the reactor load following response. Attempting to speed the response of the system to control action by increasing gains for all controllers leads to less stable behavior. The response of the reactor power to changes caused by controlling steam generator power can only occur as fast as the temperature effects can propagate through the system. Based on the dynamic response study, the speed of the reactor response to load demand changes must be limited in this control scheme to maintain stability.

The nonlinear simulation of a 10% step reduction in load demand transient provides an indication of the ability of the inherent reactor power control scheme to meet normal load following events. The design requirements for SAFR specify meeting normal load demand changes by changing power at a rate of 3% per minute within the range of 40% to 100% power. The time transient showed that this control design can better this rate for steam generator power and is only slightly less than this rate (2.7% per minute based on rise time) for reactor power. Again, reactor power lags behind the steam generator power but this is a consequence of using a passive scheme for controlling reactor power. In addition, the test simulation demonstrates the ability of this control design to meet normal load demands without causing large temperature swings in the core. The reactor mixed mean outlet temperature underwent a maximum rise of 9°F while the steady state value achieved was 6°F higher than the pre-transient hot pool temperature. The full range of control for this design can be tested in future research after specifying temperature limits for acceptability and rates of temperature change to evaluate thermal stress on the various cooling system components. The power range for inherent load following control can be determined through time response analysis and the effect of reduced flow conditions on system response time may be evaluated through further frequency analysis. No attempt was made in this study to determine the controller response to more severe duty cycle events that are beyond the range of normal load following transients. It was assumed that the plant protection system or some supervisory plant control system would use control rods to respond to such events. Given the lag between reactor power and balance of plant changes, such action would be necessary to achieve faster response or to limit the temperature swings that might result from more extreme events.

The control design presented takes advantage of the variable speed pumps available in the SAFR system configuration. However, the concept of using the inherent reactivity feedback effects to control neutron power may also be applied to other metal-fueled advanced liquid metal reactor designs. Even without flow adjustments to drive the inherent power response for load following, the behavior of reactor power given balance of plant maneuvers should allow some degree of passive control over the 40% to 100% power normal operating range, although there will likely be greater variation in system temperatures than determined in this study for this design. It is recommended that studies be performed on the EBR-II and PRISM liquid metal reactor designs to determine if similar schemes can be devised that allow the inherent neutron power behavior of metal-fueled reactors to be used to reduce the dependence on control rod insertions for power control or to act as a supplemental power control. In that case, it may be possible to decrease the required rod worth for the plant control system or define operating regimes where the control rod withdrawal may be locked out. As a result, the potential of a transient overpower without scram accident may be lessened.

Future investigations into inherent reactor power control can determine the sensitivity of the system response to changes in material and nuclear properties, core configuration, and degraded conditions to determine the potential enhancements of the feedback response that can be obtained through altered core design and to ascertain the possible degradation in response due to aging and core burnup effects. Through such work, it may be possible to tune this controller, or similar controllers for other designs, for optimum response at different power levels under different plant conditions. Accounting for the effects of aging and core burnup should allow a more detailed evaluation of the range to which inherent power control can be emphasized and a determination of the rod worth requirements for control over all conditions. In effect, as more information on the dynamic system is obtained, it will be more likely that the controller performance can be maintained under a variety of conditions. In addition, such information could be used for core design changes to enhance the favorable reactivity feedback effects to yield even more responsive inherent reactor power control.

The inherent reactor power control design for load following in SAFR developed at Oak Ridge National Laboratory represents a starting point that demonstrates the use of the inherent reactivity feedback for passively controlling reactor power in metal-fueled advanced liquid metal reactors. Modern multi-input, multi-output methods could be used to optimize its performance. However, in spite of the lag between steam-side control and reactor power response, it appears the inherent reactor power controller can meet normal load following demands in a stable, responsive manner without causing undue thermal stress within the system.

CONTENTS

Page

1.0 INTRODUCTION 1

2.0 ANALYSIS METHODS 4

2.1 SAFR Model Description 4

2.1.1 Reactor model 5

2.1.2 Hot and cold pools 8

2.1.3 Intermediate heat exchanger 9

2.1.4 Steam generator 9

2.1.5 Primary and intermediate sodium pumps 10

2.1.6 Sensors and actuators 10

2.2 Model Linearization 10

2.3 Frequency Response Calculation 13

3.0 INHERENT REACTIVITY FEEDBACK RESPONSE 14

3.1 Reactivity Effects 14

3.1.1 Fuel Temperature Effects 14

3.1.2 Coolant Temperature Effects 16

3.1.3 Structural Temperature Effects 17

3.2 Reactivity Feedback Dynamic Response 18

4.0 INHERENT REACTOR POWER CONTROL SYSTEM DESIGN . . . 32

4.1 Load and Steam Pressure Controllers 34

4.2 Core ΔT Controller 44

4.3 Intermediate Loop Controller 47

4.4 Root Locus Analysis 49

4.5 Closed-loop Performance 52

5.0 CONCLUSIONS 66

REFERENCES 70

1.0 INTRODUCTION

This report presents the work performed at the Oak Ridge National Laboratory (ORNL) to study the inherent reactivity feedback control capabilities of the metal-fueled Advanced Liquid Metal Reactor (ALMR) design concept. The objective of this work is to evaluate the feasibility of reactor power control based on thermal reactivity feedback effects and to determine the extent to which that control can be emphasized for normal load following operation. Important issues to be addressed in this task include an assessment of the behavior of the various reactivity feedback effects and their importance in affecting the desired reactor power response, an evaluation of candidate processes, other than control rod motion, for control, a determination of the dynamic response of the reactor power to actions on the selected system controllables, and an analysis of the dynamic information obtained from the reactor system to identify the limits of the inherent reactivity feedback response (or inherency) as a control issue. The results of the dynamic analysis performed are used to design an inherent reactor power controller for load following purposes during normal operation. The controller is simulated to demonstrate its transient behavior in meeting a load demand change event. Observations based on its behavior and the inherent control limits determined in this study are used to draw conclusions about the extent to which the inherent feedback response can be emphasized in a control strategy for metal-fueled ALMR load following control designs.

The current generation of ALMR designs offers enhanced inherent safety characteristics due to the configuration of the reactor system and the selected reactor materials. For both the Sodium Advanced Fast Reactor (SAFR) design [1] proposed by Rockwell International and the Power Reactor Inherently Safe Module (PRISM) design [2] submitted by General Electric, the design concept uses metallic fuel to yield more beneficial reactivity feedback behavior due to the high thermal conductivity of the material. Additional design features that promote safety include a pool configuration for SAFR, which provides significant thermal inertia, and the small modular core size of PRISM, which further enhances the negative reactivity effect caused by rod bowing. Each of these design features add to the ability of the system to safely endure a wide range of beyond design basis accident events with the thermal reactivity feedback effects providing a sufficient margin to reduce the nuclear power to prevent safe temperature limits from being exceeded. Indeed, tests demonstrating the metal-fueled LMR capability to withstand unprotected (i.e., unscrammed) loss of cooling events have been performed on the Experimental Breeder Reactor-II (EBR-II) in Idaho Falls, Idaho [3-5]. The inherent safety characteristics exhibited in these tests illustrate the significance of the inherent reactivity feedback effects for regulating power during upset

events without the benefit of control rod action. Such observations derived from the EBR-II inherent safety demonstration have led to the proposed use of the favorable inherent reactivity feedback response of metal-fueled ALMR designs, as initiated by plant action other than active control rod motion, to control reactor power during normal load following events and, possibly, during other duty cycle events [6]. Inherent reactor power control involves either active or passive use of coolant pumps and/or balance of plant (BOP) components to drive the dynamic thermal behavior that leads to the appropriate feedback response for changes in power demand. In this scheme, the goal of balancing the heat generation and heat removal in the reactor system may be achieved by altering the core temperatures through control action on the heat removal system rather than by directly controlling heat production through control rod manipulations. Thus, inherent reactor power control offers the ability to minimize control rod usage to meet various operating events. Depending on the degree to which such control can be emphasized, the potential for reducing the required worth of inserted rods to attain operating conditions can limit the degree to which rod withdrawal or ejection accidents, which may counteract some of the inherent safety features of the ALMR design, can impact plant safety. Therefore, an investigation of the inherent controllability of power in ALMRs has been performed to determine the extent to which such plants can be controlled using the intrinsic thermal feedback characteristics of the dynamic reactor system.

The Argonne National Laboratory (ANL) has recently completed an internal report [7] detailing a simulation study concerning a proposed inherent reactor power control strategy for the SAFR design. In that work, the LMR code, SASSYS (Safety Analysis System - System [8]), was used to simulate the behavior of the reactor system with the control design included. Two control strategies were evaluated. The first, a "semi-innovative" scheme, proposed using the plant control system (PCS) rods acting in concert with flow controllers to runback the plant at a controlled rate of 5%/sec in response to several of the prescribed duty cycle events for the SAFR design, described in Reference 9 as graded service conditions, rather than allowing the plant protection system (PPS) to scram the reactor. The second, an "innovative" strategy, would use no control rod action to meet duty cycle events ranging from normal load following to more severe transients (Service Conditions A to D), instead relying on pump flow and BOP temperature swings to control power in normal operation events (demand changes at 3%/min) and to runback the plant in more severe events. In both cases, certain extreme transients led to violations of the reactor temperature constraints selected for that study. From ANL's study, it seemed apparent that control rods would need to be employed to meet some of the Service Condition B through D duty cycle events (ranging from anticipated events to extremely unlikely events); however, the results did

support the feasibility of using inherency to meet the Service Condition A, normal load following events. To complement the work performed by ANL, the Advanced Controls (ACTO) program at ORNL has sponsored this study of inherent reactor power control, using time and frequency domain analysis techniques, to further investigate the possibility of meeting normal operation power requirements with the inherent reactivity feedback response of metal-fueled ALMRs.

For this study, a modular computer model of an ALMR was utilized to simulate the dynamic response of the reactor system via feedback effects to changes in controllable processes within the reactor system. The computerized whole plant model used in this study is based on the SAFR design, which was chosen as the subject reactor representative of the ALMR design concept. Given the emergence of the Integral Fast Reactor (IFR) concept [10] as a common theme in ALMR design, the configuration and core material selections that enhance the inherent safety characteristics of current designs provide for similar inherent feedback behavior. Thus, while the results of this investigation are based on the specific design characteristics of the SAFR system, the commonality of the metal-fueled ALMR inherent feedback behavior allows conclusions to be drawn about the potential of inherent reactor power control for the current proposed class of modular fast reactors.

In this work, the nonlinear model used for time domain simulation of an ALMR is also linearized and used to perform a frequency domain analysis of the system response to various controllable processes. By studying the frequency response of the open-loop system, the behavior of the reactor power as an output to a variety of inputs is evaluated to determine the desirability of using the various inputs as controllables. In addition, the frequency response of the reactivity feedback effects to flow variations and a selected time domain transient using the nonlinear model are obtained to evaluate the behavior of the various reactivity contributions in response to action on the heat removal rate in the core. The results of these analyses are used to design an inherent reactor power controller for normal load following as an example of the control design method and a demonstration of the inherent reactor power control concept. Finally, this controller is implemented using the ALMR model and its behavior during a routine load following event (Service Condition A Duty Cycle event defined over a range from 40% to 100% power) is simulated.

2.0 ANALYSIS METHODS

2.1 SAFR Model Description

The plant model for this inherent reactor power control study is the MMS-SAFR model [11] developed for the Advanced Controls program at ORNL using the Advanced Continuous Simulation Language (ACSL) [12] and the Modular Modeling System (MMS) library of reactor component modules [13]. This model is based on the SASSYS model of the SAFR plant. The MMS-SAFR version is obtained by simplifying the SASSYS formulation while maintaining the dynamic response characteristics. The simplifications include the elimination of accident analysis capabilities such as sodium boiling and fuel melt and the use of coarser mesh. Since the control system is intended to keep the plant in a safe condition, accident analysis capabilities are not needed in the control design model. The coarse mesh reduces the number of state variables thus making the MMS-SAFR more amenable to linearized state variable analysis.

Figure 2.1 shows the arrangement of the MMS-SAFR modules. The MMS-SAFR is a full plant model which can simulate all the dynamic couplings between the primary and intermediate heat transport systems and the reactor kinetics. The interactions of these systems, the time delays, and the response to control actions are the subject of the inherent reactor power control study.

The model is a one-loop model, meaning that it has a single intermediate loop model which simulates the two parallel loops operating symmetrically. For asymmetric simulation, the two loops would have to be simulated independently. Asymmetric operation is not expected to be a normal control mode. Therefore, the simpler, one-loop version is used in this control design study.

The inputs to the plant model are all the variables which can be externally controlled. The outputs are all the physical variables whose response the model simulates. The terms, inputs and outputs, can become confusing since the inputs to the plant are the outputs of the control system. For clarity, the plant inputs are referred to as "controllables". The outputs of the plant or variables which represent the measurable quantities are called the "observables".

In some cases, insight into the plant dynamics can be gained by examining the dynamic and frequency response of the some variables which are not directly measurable, such as the individual components of reactivity in the kinetics model. In Section 3, the frequency response of the reactivity components to the primary flow is examined. These plant outputs are also

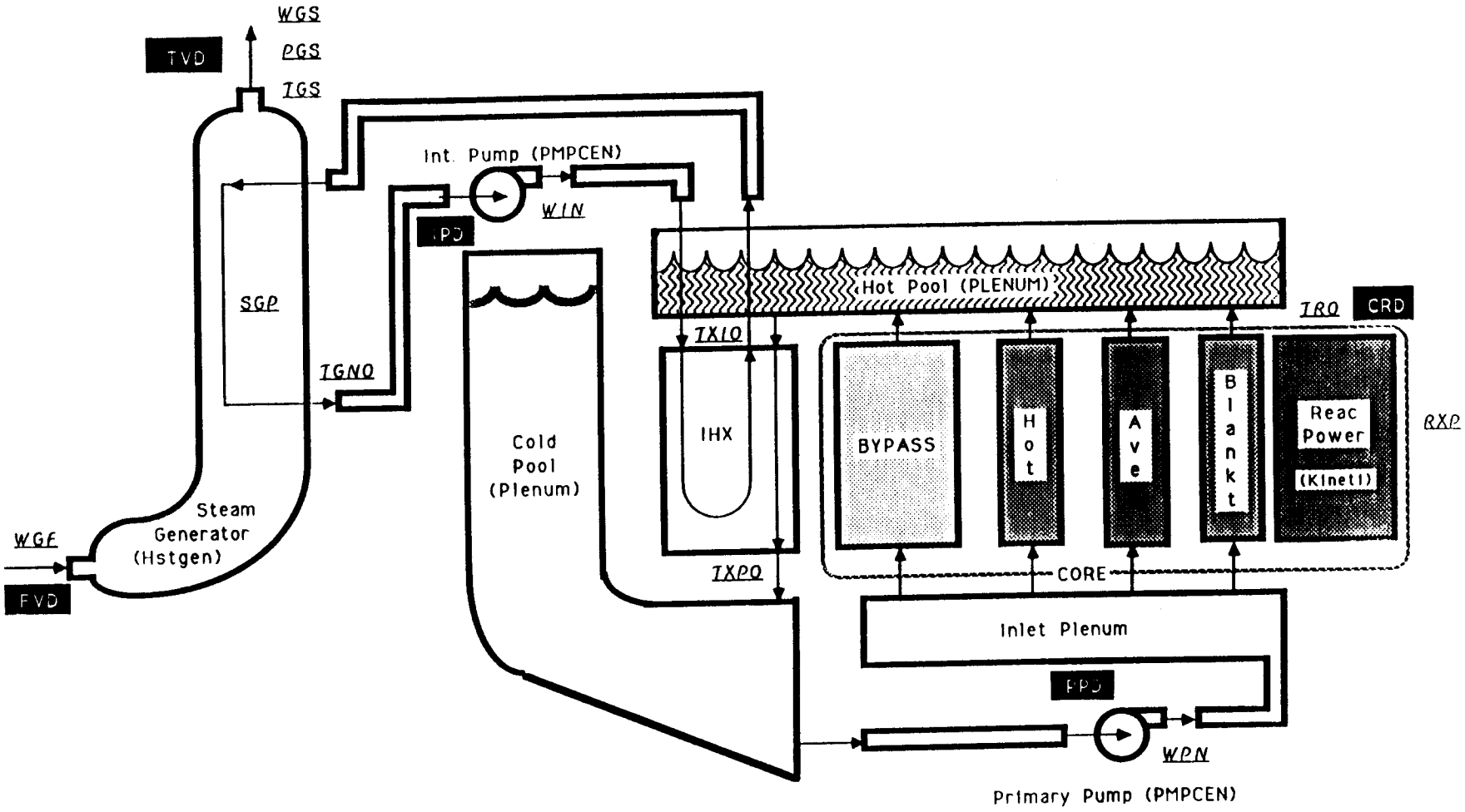

Figure 2.1 MMS-SAFR Model Schematic.

grouped with the observables. Table 2.1 lists the controllables used in this study while Table 2.2 shows the observables investigated. The controllables are shown with the system state they directly affect. The reactivity feedback effects that provide the inherent power response to thermal changes are listed with the system observables. Each controllable and measurable observable is listed with an identifier (ID) used in Figure 2.1 (controllables are shown in boxes and observables are underlined on the figure) to show the location in the model where that variable is input or calculated.

Table 2.1 MMS-SAFR Controllables

Controllables	ID	Process Affected
Control rod demand	(CRD)	Power (rod reactivity)
Primary pump motor torque demand	(PPD)	Primary loop flow
Intermediate pump motor torque demand	(IPD)	Intermediate loop flow
Turbine throttle valve position demand	(TVD)	Steam flow
Feedwater control valve position demand	(FVD)	Feedwater flow

2.1.1 Reactor model

The reactor core model represents the thermal hydraulics of the fuel pins, upper and lower structural supports, and duct wall in the SAFR core. The core design is the July 1986 End-of-Equilibrium-Cycle (EOEC), Low Burnup, Swing Design as obtained from a SASSYS SAFR data deck [14]. This is a metal fuel core and is the current design basis core for SAFR. The core model uses three channels. Channel 1 represents the peak power subassembly. The temperatures in this channel are considered the worst case for the core. The Channel 1 temperatures are compared against the operational limits for fuel, clad and coolant temperature. Channel 2 is the average driver subassembly. Channel 2 is not a particular assembly but represents the average power and flow for all driver assemblies in the core. Channel 3 is an average

Table 2.2 MMS-SAFR Observables

Measured Observables	ID	Observables
Neutron power	(RXP)	Net reactivity
Reactor outlet temperature (mixed average)	(TRO)	Coolant density reactivity
IHX primary outlet temperature	(TXPO)	Fuel/cladding axial expansion reactivity
IHX intermediate outlet temperature	(TXIO)	Fuel Doppler reactivity
SG sodium outlet temperature	(TGNO)	Radial expansion/rod bowing reactivity
Primary sodium flow rate	(WPN)	CRDL expansion reactivity
Intermediate sodium flow rate	(WIN)	Fuel Temperature
Steam flow rate	(WGS)	
Feedwater flow rate	(WGF)	
Steam temperature	(TGS)	
Steam pressure	(PGS)	
SG heat balance power	(SGP)	

blanket assembly representing the average power and flow in an internal radial blanket assembly. A bypass channel lumps together all the flow paths around the active core region. These include the coolant for the control rods and radial shields.

The reactor kinetics module calculates the neutron power, given the control rod reactivity and the feedback reactivities derived from temperatures and reactivity worths of the sodium, clad, fuel, and other structural metal. The neutron formulation uses a six precursor group, point kinetics formulation with the prompt jump approximation, which eliminates the very fast time constant associated with the neutron lifetime. The distribution of power generation is assumed to be fixed.

The decay heat is calculated using a six-term exponential approximation. The capability exists for using different decay rates for each channel. In the present analysis, the same approximation is used for all channels.

The magnitude and rate of response of the reactivity feedback are the keys to inherent reactor power controllability. The reactivity model includes components for coolant density, fuel and clad axial expansion, fuel Doppler, control rod driveline expansion, core radial expansion, and an externally controlled control rod insertion. The radial expansion includes terms representing a simplified bowing effect. The equations modeling feedback are taken directly from the SASSYS code [8]. The data representing the SAFR core design are taken from the SASSYS input deck [14]. The scope of this study of inherent reactor power control is limited to the models and core design data obtained from SASSYS.

The one significant difference between SASSYS and MMS-SAFR modeling of reactivity feedback is that the MMS-SAFR uses a much coarser mesh in the core region. The reactivity feedback depends on the distribution of temperature. A coarse distribution cannot duplicate the time response of the fine mesh exactly. However, the metal fuel and sodium coolant are very tightly linked because of the high thermal conductivities of the fuel and the coolant. As a result, the core temperatures all move in unison for slow transients. With the possible exception of the modeling of axial expansion, the low order model is quite adequate for studying inherent reactor power controllability.

The control rod worth is also included in the net reactivity calculation. Although the purpose of the study is control without rods, the frequency response of reactor and steam generator power to rod motion is useful for comparison to the other forcing functions. A simple, first order lag is used to connect the control reactivity demand to the inserted worth. The simple model is representative of the control rod drive mechanism.

2.1.2 Hot and cold pools

The pools, as shown in Figure 2.1, are passive devices that have no control inputs. The pool modeling, however, determines the primary time delay in the system. The SAFR design is a pool type reactor with large volumes at the inlet and outlet. The time constants of the hot and cold pools are 80 and 100 seconds, respectively, at full flow. The dynamic equations of the pools are developed assuming perfectly mixed tanks or, in control terminology, first order lags. At normal full flow conditions, the perfect mixing approximation is adequate. At low flow conditions not encountered in this study, laminar conditions may dominate. Disturbances or control actions initiated in the steam

or intermediate loops are filtered through these large, slow pools before they affect the core response. Several of the faster, more interesting process dynamics that are modeled are overshadowed in the actual results by the effects of the large thermal inertia contributed by these pools.

2.1.3 Intermediate heat exchanger

The intermediate heat exchanger transfers heat between the primary and intermediate loops. Considerable effort has gone into making the heat exchanger model a good low-order model simulating the heat exchanger dynamics. The description of the model order reduction and comparisons of heat exchanger models with differing order are given in Reference 11. The primary contribution of the heat exchanger to the dynamics of inherent reactor power control is through the dependence of heat transfer on flow. The flow dependence of the heat transfer equations in IHX module models the effect of flow both on the heat transfer coefficient and on the temperature distribution along the heat exchanger tubes.

2.1.4 Steam generator

The steam generator transfers heat between the intermediate steam loop and the water/steam loop. The component is modeled as a four region, moving boundary heat exchanger. Control of the overall heat removal from the plant is achieved by controlling steam and feedwater flows. These flows, in conjunction with the sodium flows, are the controllable inputs that are available for the design of an inherent reactor power control system. The boiling channel in the once-through, steam generator models the full boiling curve. The four regions in the model represent the heat transfer regimes: subcooled, nucleate boiling, film boiling and superheat. Heat removal in the once-through boiling channel with superheat contains many dependencies on region lengths, pressures, and temperatures. It is possible to have increasing sodium temperature, which decreases reactor power, while increasing steam pressure or temperature, which increases turbine power. Thus, there is a real possibility for instability due to the control strategy chosen for the steam and feedwater flows. Section 4 will describe the control schemes and controller gains that lead to instability and the gain limits for a stable control scheme. That section will also show how the maximum rate of response is limited by the maximum gains.

2.1.5 Primary and intermediate sodium pumps

The MMS-SAFR variable speed pump and motor modeling calculates the dynamics of the pump/motor from the change in demand to the actual flow change. The primary and intermediate loops of the SAFR plant are designed with variable speed sodium pumps. The flow control is one of the primary alternatives for controlling reactor power in lieu of using rod control. The ability of the system to respond to a change in flow demand is an important requirement to be considered in designing a control system. The motor torque demand is the input to the pump/motor assembly. The demand then cascades through dynamic equations for the motor torque, the shaft speed, and the sodium flow. Each stage contributes a small delay and some filtering from the input to the response.

2.1.6 Sensors and actuators

Sensor delays are not modeled for any of the observables in this model. The sensor delays are neglected because the dominant time constants in the system are much slower than those of the sensors. The slowest sensors in a plant are usually resistance temperature detectors in thermal wells, which typically have time constants on the order of three to five seconds. The dominant time constant for the primary loop is the sodium loop transit time which is approximately 200 seconds. The sensor time constants are negligible compared to the sodium loop transit time.

The dynamics of actuators such as valve positioners are not modeled for the same reason that the sensors are not modeled. One exception is the control rod drive mechanism. The drive provides the only significant delay between the neutron flux and the control rod drive demand. If the delay of the drive were neglected, the frequency response of flux with respect to control rod drive demand would have uniform gain out to infinite frequency given of the elimination of the high frequency neutron generation time effect. This is physically unrealistic so the drive mechanism is modeled as a first order lag with 0.5 second time constant.

2.2 Model Linearization

The MMS-SAFR model is a nonlinear state space model of the plant. Therefore, the plant dynamics are designed and coded as a set of ordinary, first order,initial value differential equations. Formally, the state space model can be written as two vector functions, such that

$$\dot{\underline{x}} = F(\underline{x}, \underline{u}, t) \tag{2-1}$$

and

$$\underline{y} = M(\underline{x}, \underline{u}) \tag{2-2}$$

where $\dot{\underline{x}}$ is the derivative vector,
$\underline{x}$ is the state vector,
$\underline{u}$ is the input vector (controllables),
$\underline{y}$ is the output vector (observables),
$\underline{F}$ is the derivative function,
$\underline{M}$ is the observation function, and
t is time.

The MMS-SAFR model is coded so that it calculates these functions explicitly. The coding produces single vector values for the current time. The results do not depend on the arguments (state and control vectors) at any previous time. The calculation can be made without any internal iterations or previous values.

Although there are some advances in nonlinear control analysis and design methods, the majority of control theory and analysis is based on linear systems. Linearization is always an approximation to the true dynamics, but the approximation is frequently acceptable and is justified by the computational efficiency advantage over nonlinear methods and by the additional insight one can gain from the methods of linear system analysis.

The linear state space model has the following form:

$$\dot{\underline{x}} = \mathbf{A}\underline{x} + \mathbf{B}\underline{u} \tag{2-3}$$

and

$$\underline{y} = \mathbf{C}\underline{x} + \mathbf{D}\underline{u}\,, \tag{2-4}$$

where $\underline{y}$, $\underline{x}$, and $\underline{u}$ have the same meaning as before, and **A**, **B**, **C**, and **D** represent the coupling between state variables, state derivatives, controllables, and observables. In the linearized state space model, the elements of **A**, **B**, **C**, and **D** can be written as partial derivatives giving

$$A_{i,j} = \frac{\partial \dot{x}_i}{\partial x_j}\,, \tag{2-5}$$

$$B_{i,j} = \frac{\partial \dot{x}_i}{\partial u_j}\,, \tag{2-6}$$

$$C_{i,j} = \frac{\partial y_i}{\partial x_j} , \tag{2-7}$$

and

$$D_{i,j} = \frac{\partial y_i}{\partial u_j} . \tag{2-8}$$

The explicit functional form of the MMS-SAFR model makes it particularly easy and accurate to calculate the linearized system matrices numerically. The partial derivatives are calculated by perturbation as follows,

$$A_{i,j} = \frac{1}{2\Delta x}[F_i(x_1,\ldots,x_j + \Delta x_j,\ldots,x_k,\underline{u},t) - F_i(x_1,\ldots,x_j - \Delta x_j,\ldots,x_k,\underline{u},t)] , \tag{2-9}$$

$$B_{i,j} = \frac{1}{2\Delta u}[F_i(\underline{x},u_1,\ldots,u_j + \Delta u_j,\ldots,u_n,t) - F_i(\underline{x},u_1,\ldots,u_j - \Delta u_j,\ldots,u_n,t)] , \tag{2-10}$$

$$C_{i,j} = \frac{1}{2\Delta x}[M_i(x_1,\ldots,x_j + \Delta x_j,\ldots,x_k,\underline{u},t) - M_i(x_1,\ldots,x_j - \Delta x_j,\ldots,x_k,\underline{u},t)] , \tag{2-11}$$

and

$$D_{i,j} = \frac{1}{2\Delta u}[M_i(\underline{x},u_1,\ldots,u_j + \Delta u_j,\ldots,u_n,t) - M_i(\underline{x},u_1,\ldots,u_j - \Delta u_j,\ldots,u_n,t)] . \tag{2-12}$$

The linearization calculation is a built-in function of the ACSL simulation language. It is called via the ANALYZ "JACOB" command. The only problem experienced during this study with the numerical linearization was the need to increase the perturbation step size from the default value in order to avoid inaccuracy in coefficients, which affected primarily the low (near steady state) frequency response. The output of the ACSL linearization can be written in a file format that can be read directly by the Matrix_x engineering analysis and control design program [15], which is the matrix analysis package used for the frequency response calculations performed in this work. The convenient data transfer is important for this effort since the system state matrix composed of **A**, **B**, **C**, and **D** has dimensions as great as 148 by 153.

2.3 Frequency Response Calculation

The frequency response plots or Bode plots relate the gain (ratio of output to input) and phase shift (the time delay between the output and input) to frequency and are representative of the dynamic response of the system to sinusoidal input signals to the plant at the various frequencies. The phase and gain plots for linear systems can be directly calculated from the system transfer functions, which are obtained from the linearized system matrices. Taking the Laplace transform of the linearized state space model (Eqs. 2-3 and 2-4) with zero initial conditions and undergoing various matrix manipulations yields a matrix equation for the ratio of observables to controllables in terms of a resolvent or characteristic matrix, $(s\mathbf{I} - \mathbf{A})^{-1}$, and the other state space matrices. The ratio elements of this matrix represent the single-input, single-output transfer functions between the various observable/controllable combinations. The frequency response of each observable to perturbations in selected controllables is obtained directly from the transfer function matrix by substituting $j\omega$ for the Laplace variable. Thus, the gain and phase of the frequency response of an observable to a controllable is determined by the poles (the zeros of the resolvent matrix determinant) and the zeros of the appropriate transfer function. The phase shift and magnitude of each response are determined by purely numerical evaluations from these matrix elements involving complex arithmetic. Matrix_x has a standard function which calculates the frequency response from the linearized state space matrices. The utility, called BODE, transforms the state space matrices into the transfer function matrix and evaluates the gain and phase of the transfer function numerically.

3.0 INHERENT REACTIVITY FEEDBACK RESPONSE

The prompt negative net reactivity feedback in metal-fueled ALMR designs provides an inherently safe response during loss of cooling events. This behavior results from the combined effect of various temperature-driven reactivity feedback components whose desired characteristics have been enhanced in current metal-fueled LMR designs [16-19]. The reactivity feedback effects studied include the fuel Doppler effect, the coolant density effect, the fuel/cladding axial expansion effect, the control rod driveline (CRDL) expansion effect, and the core radial expansion/thermal bowing effect. All the reactivity effects, except for the coolant density feedback, are negative for an increase in temperature. The choice of fuel type in the ALMR design most strongly affects Doppler resonance broadening and fuel/cladding axial expansion. The higher thermal conductivity of the metal fuel causes the fuel temperature to respond faster to heat production and removal changes while leading to lower centerline temperatures than for oxide fuel. Also, the sodium void reactivity worth is made more positive due to the harder neutron spectrum that results from metallic fuel. The other reactivity effects can be classified as being dependent on structural temperatures and are not directly affected by fuel type. The intrinsic feedback behavior of metal-fueled LMRs provides the mechanism by which inherency is achieved. By understanding the response of the net reactivity feedback and its component effects to alterations in the system state through flow or temperature variations, the inherent reactor power control characteristics of the ALMR design can be evaluated.

3.1 Reactivity Effects

3.1.1 Fuel Temperature Effects

Inherent reactivity effects respond to the thermal behavior of the reactor core components (i.e., fuel, coolant, and structural temperatures). The fuel temperature is primarily determined by the reactor power density and the thermal conductivity of the fuel and cladding material. In addition, the coolant and clad temperatures affect the fuel temperature via their influence on the heat removal rate in the core. The fuel Doppler and fuel/cladding axial expansion feedback effects are dependent on the fuel and cladding temperatures. The behavior of these reactivity effects is determined by the nuclear, thermal, and mechanical properties of the chosen metallic fuel.

The fuel temperature reactivity effect resulting from Doppler broadening of resonances in the absorption cross section due to thermal motion of the fuel material nuclei leads to a prompt decrease in reactivity with increasing fuel temperature. The

Doppler reactivity is proportional to the logarithm of the fuel temperature with a negative feedback coefficient. Since the reduction in scattering collisions due to coolant voiding affects the neutron spectrum at the fuel absorption resonance energies, the Doppler reactivity is calculated using the full-channel and voided-channel Doppler coefficients, weighted by the coolant density. For a metal fuel core, the neutron spectrum is harder due to the lack of moderating oxygen in the fuel material. As a result, the Doppler reactivity coefficient is less negative than for an oxide-fueled core. The high thermal conductivity of the metal fuel provides a moderate temperature gradient across the fuel, thus allowing the average fuel temperature to respond more quickly to coolant changes. The metal fuel response to a change in heat removal will be a larger prompt change in fuel temperature than for oxide fuel so, in spite of the smaller Doppler reactivity coefficient, the immediate fuel thermal reactivity effect for a metal core is very similar to that of an oxide core. Thus, in the short term, the higher conductivity of a metal fuel compensates for the lower reactivity coefficient. For large power reduction events, the moderate thermal gradient in the metal fuel limits the positive reactivity effect of a cooling core since, as the temperature profile becomes more uniform, the drop in average fuel temperature is less dramatic than for oxide fuel with its much larger difference between centerline and surface fuel temperatures. Thus, for inherent reactor power control purposes, the reactivity contribution of the Doppler effect as a power maneuvering transient progresses will be in opposition to the desired net reactivity effect (e.g., a positive Doppler reactivity contribution for a desired power reduction over time), however, its effect will be less pronounced that the comparable effect for an oxide-fueled core.

While the thermal conductivity of a metal core strongly influences the fuel Doppler feedback behavior, the thermal expansion characteristics affect the fuel/cladding axial expansion reactivity contribution. As the fuel elements expand axially, the fuel is spread over a larger area, thus reducing the density of fissile material in the active core. Hence, the fuel worth in the expanded core is less. As fuel temperature increases and the fuel expands axially, its reduced worth yields a negative reactivity contribution. Conversely, fuel/cladding contraction leads to a positive reactivity effect. The expansion of the cladding material yields a positive reactivity effect but it is much smaller in magnitude than the accompanying negative effect caused by fuel expansion. The axial expansion reactivity is calculated using the thermal expansion characteristics of the cladding material to determine if the fuel length change is impeded by slower cladding expansion or is free to change at its own rate without restriction. The overall reactivity feedback coefficient for this effect is negative. The thermal expansion coefficient for metal fuel is roughly double that of oxide fuel so, given the limits imposed by cladding expansion, metal fuel expands or

contracts significantly more due to fuel temperature changes than does oxide fuel. For loss of cooling or flow reduction events, the axial expansion effect provides negative reactivity due to increased fuel temperatures. As a result of this behavior and the Doppler reactivity contribution, the power density in the core decreases and the heat production is reduced, thus leading to fuel contraction and a positive long term reactivity contribution. As is the case for Doppler reactivity, this behavior provides the favorable prompt reactivity effect, but it also acts against the desired long term feedback response for inherent neutron power control via heat removal manipulations. Therefore, during power reductions, other feedback effects must account for the effects of Doppler and axial expansion as fuel temperature drops to allow power control by altering the heat removal rate.

3.1.2 Coolant Temperature Effects

The coolant temperature determines the behavior of the coolant density reactivity effect. For a moderate-sized sodium reactor, the coolant density feedback coefficient is negative (i.e., the core has a positive sodium void worth). Sodium expansion due to increased coolant temperature lowers the probability of neutron absorption in the coolant channel and, thus, increases the likelihood of fission absorptions in the fuel. The accompanying reduction in scattering has been previously described in terms of its effect on the Doppler reactivity. These effects are enhanced by the harder neutron spectrum in a metal core. The sodium density reactivity feedback is calculated by determining the sodium void fraction and multiplying by the void worth. Increasing coolant temperature by altering the heat removal process in the reactor system causes a fast, positive coolant density reactivity effect. This effect is soon joined by the positive reactivity effects of the fuel Doppler and fuel/cladding axial expansion feedbacks after the power has decreased (and fuel temperature dropped) due to the prompt negative behavior of the overall reactivity. Thus, for short term behavior during transient conditions, the coolant density effect runs counter to the desired net inherent reactivity response. However, as the coolant loop cools in response to the resultant lowered heat generation, the long term contribution of the coolant density feedback is negative reactivity. The coolant density reactivity provides a detrimental contribution to prompt inherent power control but becomes an important beneficial effect as power stabilizes in the long term.

3.1.3 Structural Temperature Effects

Changes in the coolant temperature lead to changes in structural temperatures in the reactor system. As the temperature of a control rod assembly changes, it expands or contracts in response. As a result, the control rods themselves are inserted or withdrawn small amounts as the control rod driveline expands or contracts. The core outlet coolant temperature washes the control rod driveline, so increases in the sodium temperature cause a negative reactivity insertion by the expanding control rod assemblies. CRDL reactivity is determined by the temperature change in the coolant, the thermal inertia of the control rod structure, and the thermal expansion coefficient of the assembly. The magnitude of the effect depends on the control rod worths and their location in the core. The effect can be reduced by the action of vessel expansion of the support structure. As the vessel expands, the control rod drive supports may be raised or the core may be lowered, thus slightly withdrawing the control rods. However, considering the mechanical restraints on the vessel and its larger thermal inertia (as well as the cooling provided by the cold pool for the SAFR configuration), this effect is relatively small and will not be included in this study. Therefore, the CRDL reactivity effect will provide a negative feedback contribution to flow or cooling reduction events; however, the effect will be delayed slightly as the temperature rise reaches the control rod driveline and heats the assemblies. This reactivity effect helps provide the desired inherent response for both safety and control considerations but its impact is delayed.

The radial expansion/thermal bowing reactivity effect is provided by structural thermal behaviors that evolve on different time scales. Thermal bowing is stimulated by the change in core coolant temperatures and temperature gradients that result from altered heat removal in the core. This effect occurs shortly after the onset of transient conditions. As the assembly duct walls heat and expand at the upper core load pads, the relative position of the core assemblies changes in the upper regions of the core. This opening of the spaces between the fuel assemblies high in the core is known as core flowering. More constrained upper support configurations lead to bowing of the fuel assemblies. The movement of fuel and steel causes a negative reactivity effect due to the reduction of fissile material density. The moderately fast duct wall expansion and the constraints on the core assemblies determine this structural thermal effect. For small cores with free flowering core designs, this effect can be strongly negative. Radial expansion is dominated by the grid plate expansion, which evolves on the much slower time scale needed to heat (or cool) the lower support structure. Radial expansion of the core leads to a uniform decrease in fuel density and, thus, a negative reactivity effect. The loop time of the primary coolant strongly influences the delay

in this effect. The expansion reactivity is based on the thermal changes in the lower support which depends on the core inlet temperature. The thermal bowing feedback provides a large negative reactivity for loss of cooling and inherent power control maneuvers such as flow reductions while the radial expansion effect depends strongly on the slower behavior of the inlet coolant temperature. The prompt behavior of the core thermal reactivity effect is very important in providing the desired inherent feedback behavior for both safety and control.

Inherent reactor power control depends on causing an in-phase change in power for a change in core cooling, either through flow or temperature variations. The described reactivity feedback effects provide this behavior as a group in response to upset events. On different time scales, the contribution of each is varied; nonetheless, the net effect provides negative reactivity for reduced heat removal (e.g., higher coolant temperatures) to lower the heat production or gives positive reactivity for increased heat transfer (e.g., more coolant flow) to raise reactor power. The key to enabling inherent reactor power control is to perturb the appropriate process(es) to ensure that the inherent feedback response acts rapidly enough and without large swings in the system state to meet normal duty cycle demands. In addition, the long term response of the reactivity components, some of which are strongly affected by the inlet coolant temperature behavior, determines the degree to which steady state power can be changed as the overall reactivity approaches an equilibrium condition. Therefore, the dynamic response of the reactivity effects to inherent control processes needs investigation.

3.2 Reactivity Feedback Dynamic Response

The dynamic response of the ALMR reactivity feedback should be studied in both the time domain through transient simulations and in the frequency domain using frequency response techniques on the system model. For this study, the open-loop frequency response of each reactivity feedback effect to a control of the heat removal rate in the core was obtained from a linearized system model generated by ACSL using the MMS-SAFR code. This linear analysis allows determination of the net reactivity response to primary flow changes, which represent the most direct means of altering core heat removal. The results of this analysis are used to assess the prompt, short term and long term contributions of each reactivity component that result from perturbations in primary coolant flow and, thus, in the core thermal condition. Additionally, a time transient simulating a step change in primary flow demand is presented to support the conclusions about the inherent reactivity behavior drawn from the frequency response analysis. From these observations, the types

of flow and temperature control needed to cause and maintain a neutron power change can be evaluated.

The linearized model of the SAFR plant was generated with primary pump demand (and thus, primary flow) as the controllable, while the net reactivity and its component contributions (coolant density, axial expansion, Doppler, radial expansion, and CRDL expansion reactivities) were specified as observables. The model configuration used in this investigation of the reactivity behavior consists of the full plant through the water side of the steam generator. The feedwater and steam flow boundary conditions are pressure dependent while the feedwater temperature is fixed. The analysis results reflect the response of the open-loop system without any external control action within the system. The model was linearized at 100% power and 100% flow steady state conditions for the previously described EOEC core configuration. The reactivity feedback responses are presented in this section as Bode plots showing the frequency dependent magnitude and phase of the transfer function between each reactivity effect and the control variable, primary pump demand. The units of the transfer functions are dollars of reactivity per unit pump demand change with the pump demand normalized to one at full flow conditions.

Before discussing the reactivity feedback dynamics, the effect of modeling assumptions on the frequency responses presented in this section should be addressed. The linearization process occurs at a steady state condition and the resulting linear model cannot describe any nonlinear effects within the model or the physical system being modeled. The assumption is that the model behavior is not strongly nonlinear. As it turns out, the calculation of the fuel/cladding axial expansion reactivity effect in the MMS-SAFR code (as derived from SASSYS) changes as the model state undergoes a discontinuity in the reactivity worth from fuel expansion beyond its initial noding size to contraction below its original noding. The discontinuity is clearly not a physical effect and is related to the formulation used. The finer axial mesh employed in SASSYS may minimize this effect but the coarse mesh used in MMS-SAFR yields a noticable discontinuity. Each condition yields its own frequency response (Figure 3.1). The linearized expansion response has a larger gain than the contraction response over all frequencies and it approaches zero phase at low frequencies as opposed to the out-of-phase behavior for contraction. Obviously, the frequency response obtained depends on the starting point at which the model was linearized and it cannot account for the nonlinear transition.

The differences between the two axial expansion formulations has very little effect on the other feedback dynamic responses above 0.01 rad/s (other than slightly increasing the gain of the net reactivity). It is only in the low frequency region (below ~0.006 rad/s) that the frequency responses of the other feedback effects change significantly under the two axial expansion

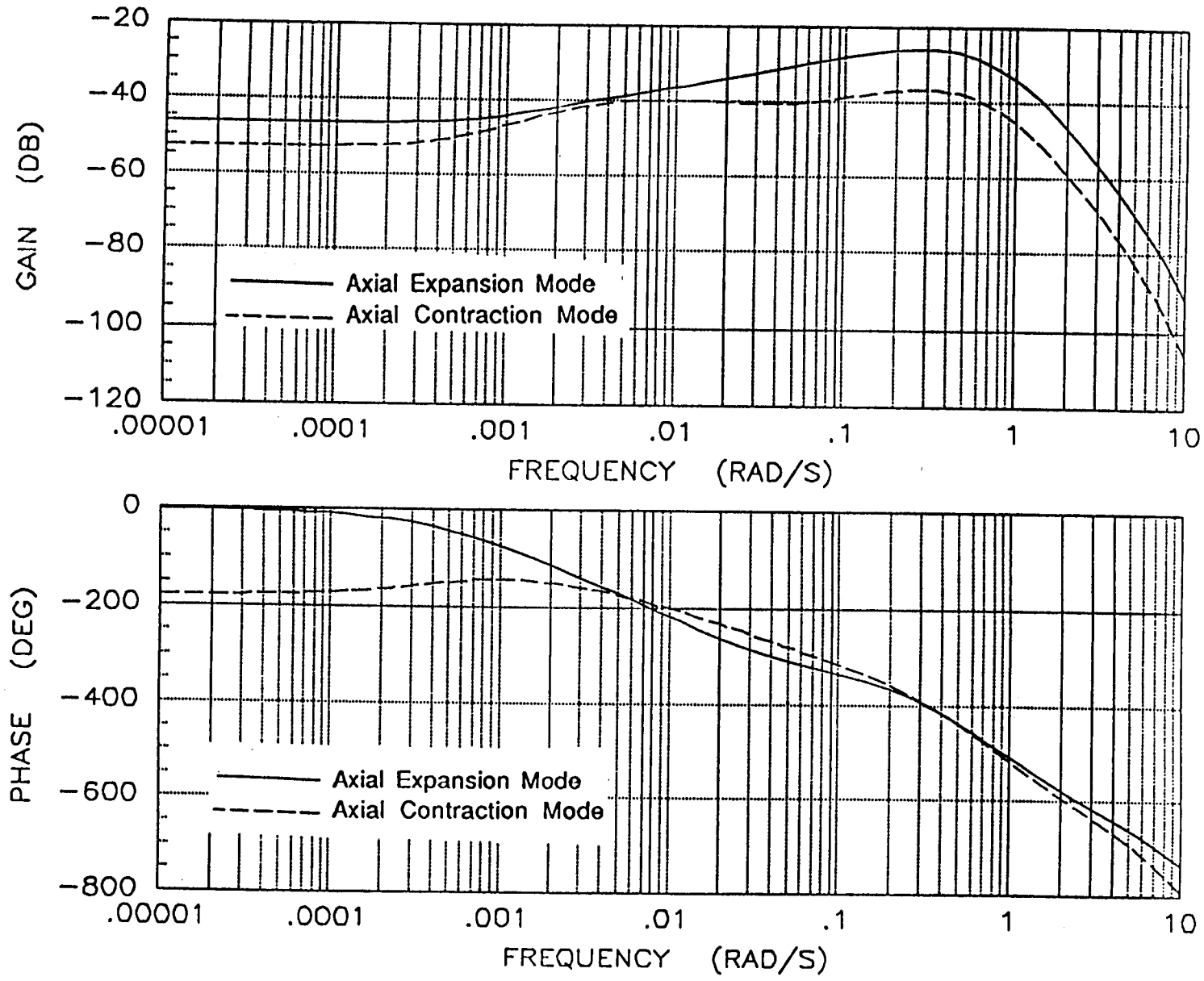

Figure 3.1 Axial Fuel Thermal Reactivity Effect: Comparison of Expansion Mode Frequency Response with Contraction Mode Frequency Response.

conditions. The gains for the coolant density and radial expansion effects are higher for the response with the axial expansion formulation while the Doppler and CRDL expansion reactivity gains are lower. The phase behavior of the other reactivity feedbacks does not change appreciably. This low frequency difference in gain is expected since the long term trend of each effect is to seek equilibrium with the other reactivity feedbacks to lead overall reactivity to zero. Thus, a change in the behavior of one feedback affects the behavior of the other reactivity components in the long term. For a reduction in flow, the middle and high frequency response of the expansion formulation gives the expected axial expansion feedback behavior as the fuel expands with increased temperature then contracts to its original length. From Figure 3.1, it can be seen that the phase behavior of the contraction mode approaches -180° at low frequencies. This provides the expected low frequency response to the decreased fuel temperature that would result from a flow reduction transient. The differences in the low frequency behavior of the other feedbacks can be described by ranking their gains. The coolant density gain is nearly -30 dB, radial expansion is approximately -33 dB, Doppler is -40 dB, CRDL expansion is about -47 dB, and axial expansion approaches -50 dB. The gain for net reactivity decreases rapidly toward -100 dB at low frequencies.

Given the similarity in the middle and high frequency ranges of the feedback responses for the two axial thermal behavior calculational modes, the short term reactivity behavior may be evaluated in spite of the nonlinear component of the model. In addition, the long term contraction mode responses for the various feedback effects appear to be representative, at least qualitatively, of their expected behavior below approximately 0.006 rad/s. Therefore, the results from the linear frequency analysis can still provide insight into the short term behavior of the feedback effects and their long term responses. While the errors introduced by the modeling discontinuity appear to be managible since the long term axial expansion effect is small relative to other feedback effects, further study into the sensitivity of the frequency response results to modeling approximations (and to parametric changes caused by aging and fuel burnup) should be performed in future work.

Given these considerations, Figures 3.2 and 3.3 show the frequency responses of the overall and component reactivity effects to primary flow perturbations. The net reactivity is shown to be most responsive to changes in primary flow in the middle frequency range (~0.03 rad/s to 1.0 rad/s) with its highest gain occurring near 0.2 rad/s. The gain of the net reactivity to primary pump demand transfer function drops considerably outside of this frequency band. As a result, the response of the net reactivity to a core flow transient is most pronounced for changes within that frequency band. For an abrupt flow change, the net

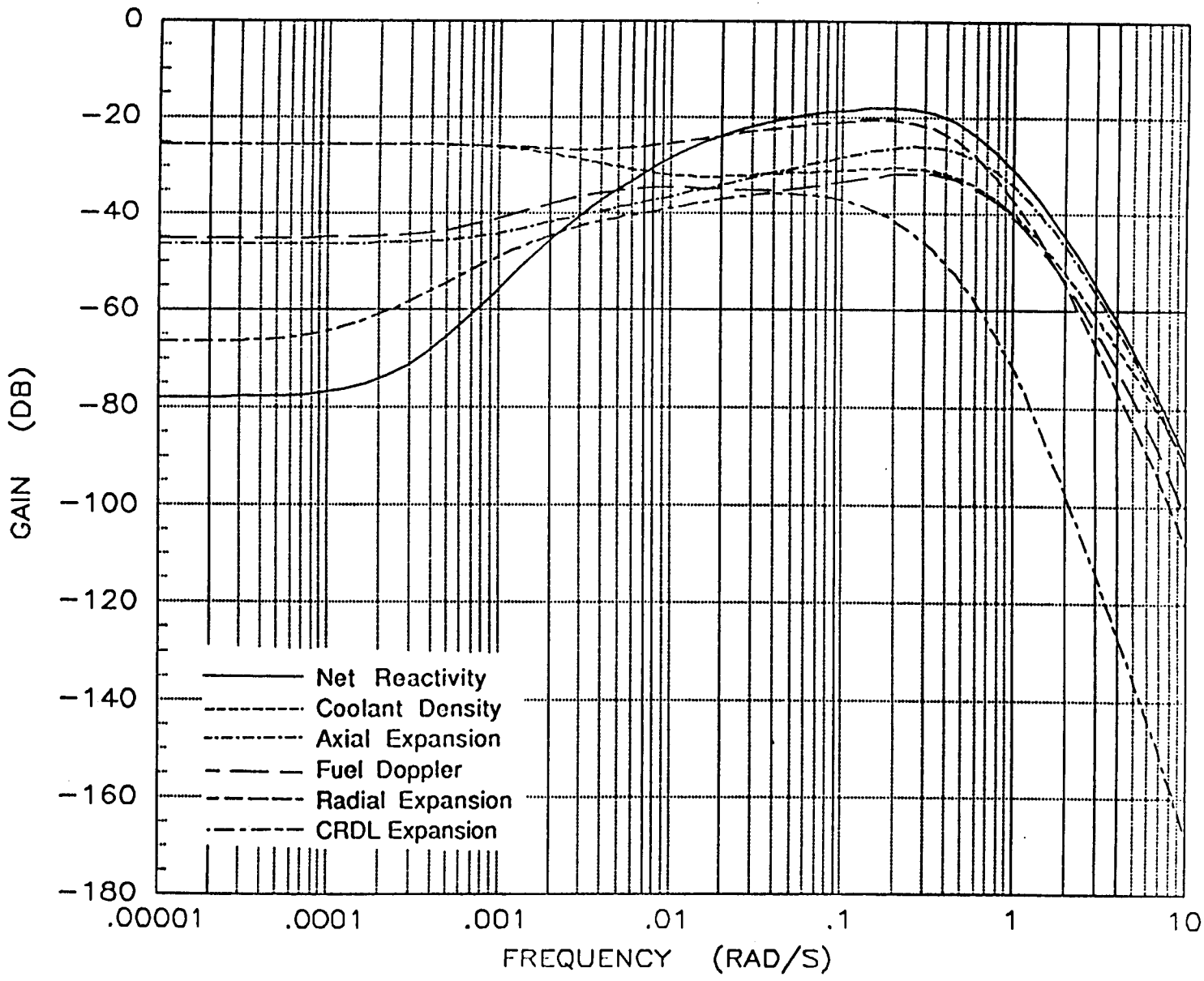

Figure 3.2 Reactivity to Primary Flow Frequency Response Gains.

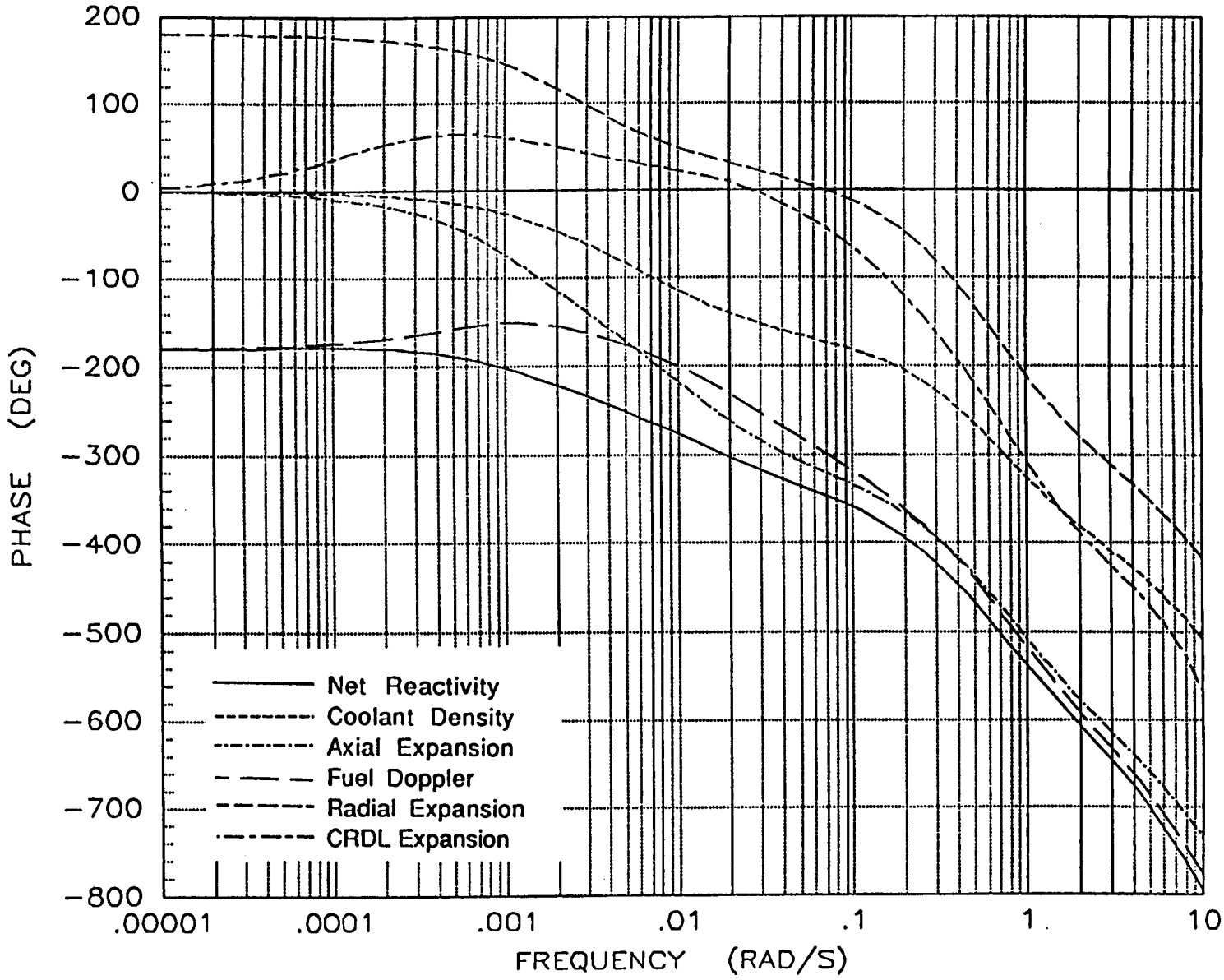

Figure 3.3 Reactivity to Primary Flow Frequency Response Phase Relations.

reactivity would undergo its greatest rate of change early in the transient. Based on the location of the maximum gain, the peak value of the net reactivity should occur promptly following a flow change with the reactivity effect being of the same sign as the flow perturbation. The inherent stability of reactor power is such that the reactivity feedback, in response to a change in flow, seeks equilibrium and brings the net reactivity to zero in the long term (i.e., approaches $-\infty$ dB at low frequency). Thus, the magnitude of the net reactivity to primary pump demand transfer function decreases rapidly at low frequencies as the power approaches a new steady state. Over the frequency range where the gain is significant, the net reactivity is essentially in-phase with the flow perturbation so a decrease in flow leads to a negative reactivity effect. At lower frequencies, the response becomes out-of-phase with a small gain, indicating a slightly positive reactivity as the power stabilizes. Therefore, with no other action taken on the system, a decrease in core flow should lead to a large prompt negative reactivity effect which will be reduced until the reactivity goes slightly positive later in the transient. The magnitude of the net reactivity will slowly decrease as it approaches zero in the long term. The power should be reduced by a large amount quickly and then rise slowly to some new steady state value less than its original value. The likely cause for this behavior is the dominance of the large prompt negative reactivity effects early in the transient followed by the gradual cooling of the reactor system temperatures with reduced power, leading to less negative and eventually positive reactivity contributions from several component feedback effects. The behavior of the individual reactivity feedback effects illustrate the system dynamics that lead to the net reactivity response.

The coolant density, fuel/cladding axial expansion, and fuel Doppler reactivity feedback effects have similar gains in the middle frequency range, with break frequencies of approximately 0.5 to 0.6 rad/s. Thus, these reactivity effects respond promptly to a flow change, with coolant density reactivity leading slightly given its slower decrease in gain at the higher frequencies. The phase behavior of these three effects indicates that the prompt response of the coolant density reactivity is opposite to that of the other two, and of opposite sign with the flow change. Between 0.04 and 0.004 rad/s, all three effects are essentially in-phase with each other and out-of-phase with flow. The coolant density achieves an in-phase behavior with flow below this range. Thus, with decreased flow, the coolant density will decrease with increased coolant temperature as the coolant heat transport from the core is reduced, leading to a positive reactivity change. The axial expansion and Doppler effects will follow the flow change promptly as fuel temperature changes quickly with altered heat removal given the high thermal conductivity of the metal fuel. The reduced power, caused by the prompt negative net reactivity, lowers the fuel temperature so that the axial expansion and Doppler contributions become less negative. Some short time

following a flow reduction, both fuel reactivity effects will become positive as the fuel cools below its original state due to reduced reactor power. This is indicated by the phase transition in the 0.03 to 0.05 rad/s region. The cooling of the reactor system leads the coolant density effect to become negative as the average coolant temperature drops in the long term. Again, this behavior is indicated by the coolant density phase behavior in the 0.004 to 0.008 rad/s frequency region. As a result, in the short and long term, the coolant density reactivity feedback acts in opposition to the reactivity contributions of the Doppler and axial feedbacks (based on the low frequency phase behavior of the axial contraction mode). Initially, the coolant density is out-of-phase with a flow change, and thus is opposing the desired inherent power control response. However, over the long term behavior of a primary flow transient, the coolant density effect acts in a beneficial manner by providing an in-phase reactivity contribution with the largest steady state gain.

The radial expansion/rod bowing reactivity effect provides the largest gain in the middle frequency range where overall reactivity is most responsive to flow changes. The early response of this reactivity effect is caused by core flowering due to increased coolant temperature at the upper duct walls. Its break frequency (~0.4 rad/s) is less than that of the coolant density, fuel/cladding axial expansion, and fuel Doppler reactivities and its peak gain is very close to that of net reactivity in magnitude, occurring at about 0.15 rad/s. Therefore, the radial expansion feedback (dominated by rod bowing) should peak quickly after a flow change, with a response time slightly longer than that of the other three effects, and have a large in-phase reactivity contribution. The phase relation of the radial expansion/row bowing feedback changes at around 0.002 rad/s such that its long term contribution is out-of-phase with the flow change. This change probably results from the delayed effect of grid plate expansion. As the coolant loop temperatures drop during a flow reduction transient, the large mass of the lower grid support plate contracts and the fuel is brought into a slightly more compact configuration. This provides a positive reactivity effect due to the higher fissile material density. Again, this long term behavior is contrary to the desired net response but the cooling trends that lead to this effect also provide the negative, long term contribution by the coolant density reactivity. This total behavior illustrates the inherent stability of the reactivity effects in the long term since, as temperatures change to produce one reactivity effect, other temperatures change to cause reactivity effects that counteract that response so that power reaches a new steady state.

Finally, the delay in the CRDL expansion reactivity contribution is apparent from the gain plot. The break frequency of the CRDL effect is approximately 0.2 rad/s with the peak gain occurring at nearly 0.05 rad/s. Therefore, the response time of the CRDL expansion effect is longer than that of the other effects

and the rapid drop off in gain at high frequencies indicates very little response in this reactivity immediately following the initiation of a flow change event. Thus, the biggest contribution from this reactivity occurs later in a flow transient. Of course, this delay results from the time required for the hotter coolant to reach the control rods and heat the assemblies sufficiently for expansion during a flow reduction transient. The CRDL expansion effect is essentially in-phase with flow throughout a transient. This indicates that the outlet coolant temperature remains higher than its original state as the reactor reaches a new steady state following a flow reduction. Therefore, although the inlet temperature drop reduces the average coolant temperature and gives a negative coolant density effect in the long term, the core outlet temperature seeks a slightly higher post-transient steady state to yield a small negative CRDL expansion contribution as the transient settles.

The frequency response can be used to predict the time behavior of the system to a step forcing function. The transfer function in that case describes the rate of change for the time response. The shape of the frequency response is a result of the dominant zeroes and poles of the transfer function. For second order systems, characterized by a resonance peak, the magnitude of the resonance estimates the peak value of the time transient and the resonance frequency provides a relative indication of the transient time response of the system. For systems with a damping ratio greater than 0.4 (i.e., a less sharp resonance peak), there is a close correlation between the resonance gain and the peak time value. For systems of higher than second order, the step response of the system can be analyzed in terms of an effective damping and natural frequency with additional exponentially decaying terms resulting from real poles. A sample flow transient was simulated using the nonlinear MMS-SAFR model to provide time response data for comparison with the observations derived from the frequency response analysis. By such a comparison, the assumptions involved in the linearization process can be evaluated and the effect of the axial expansion reactivity worth discontinuity can be seen.

The flow transient chosen is a 25% step reduction in primary pump demand from 100% flow following a 10 second null transient. Figure 3.4 shows the short term behavior of the net reactivity and its component effects while Figure 3.5 gives the long term response of the reactor system to the flow step with no other action taken on the heat removal process. As was deduced from the frequency response of the net reactivity, the flow reduction leads to a prompt negative reactivity change with its highest rate of change occurring in the first 30 seconds of the transient. The almost -$0.033 overall reactivity value corresponds to a -17.6 dB gain (~$0.132/pump demand change) for a 25% step reduction in flow demand, which is approximately that observed in the frequency plot. The net reactivity becomes slightly positive after 160 seconds as

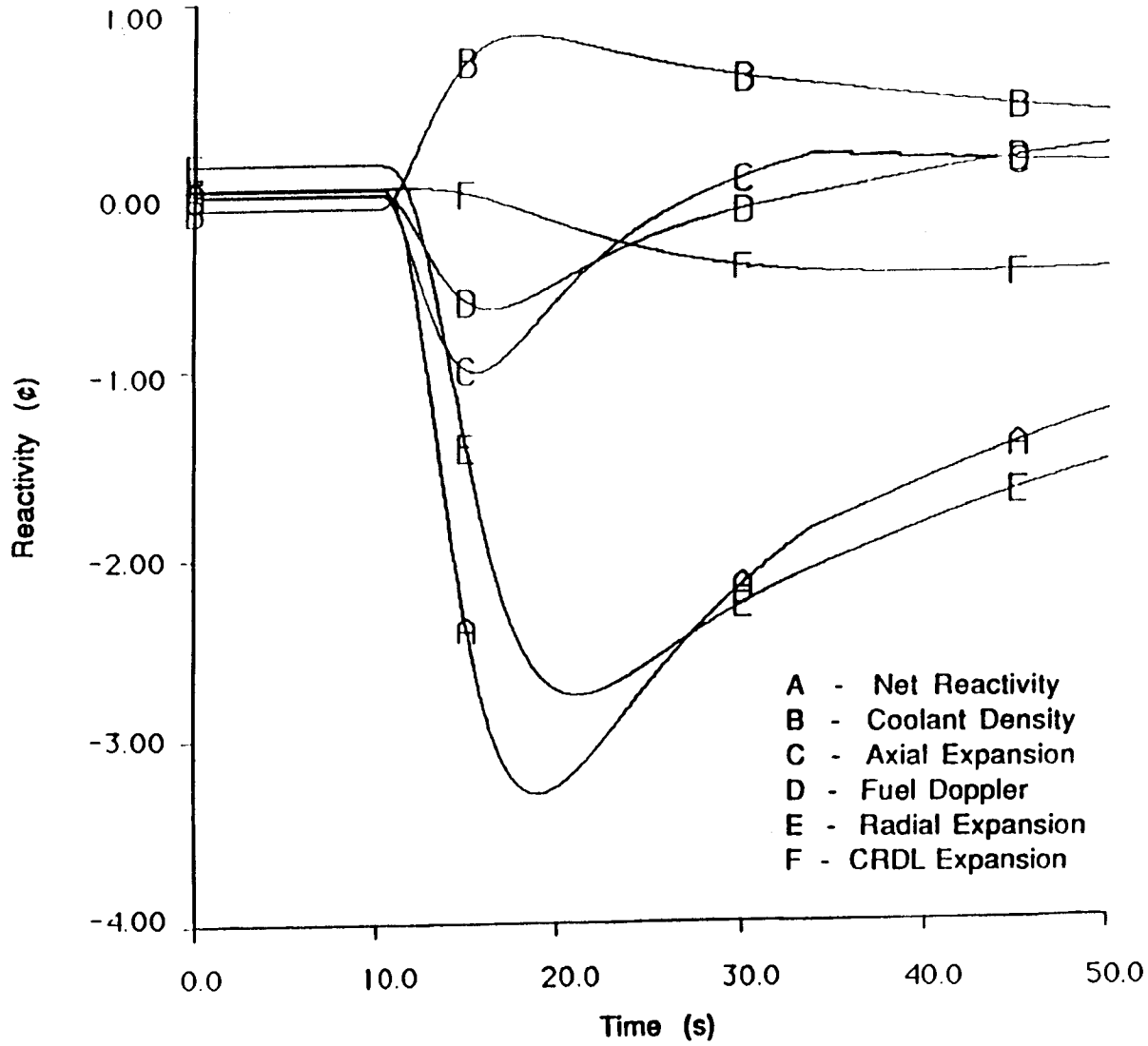

Figure 3.4 Prompt Reactivity Effects For 25% Step Reduction In Primary Pump Demand.

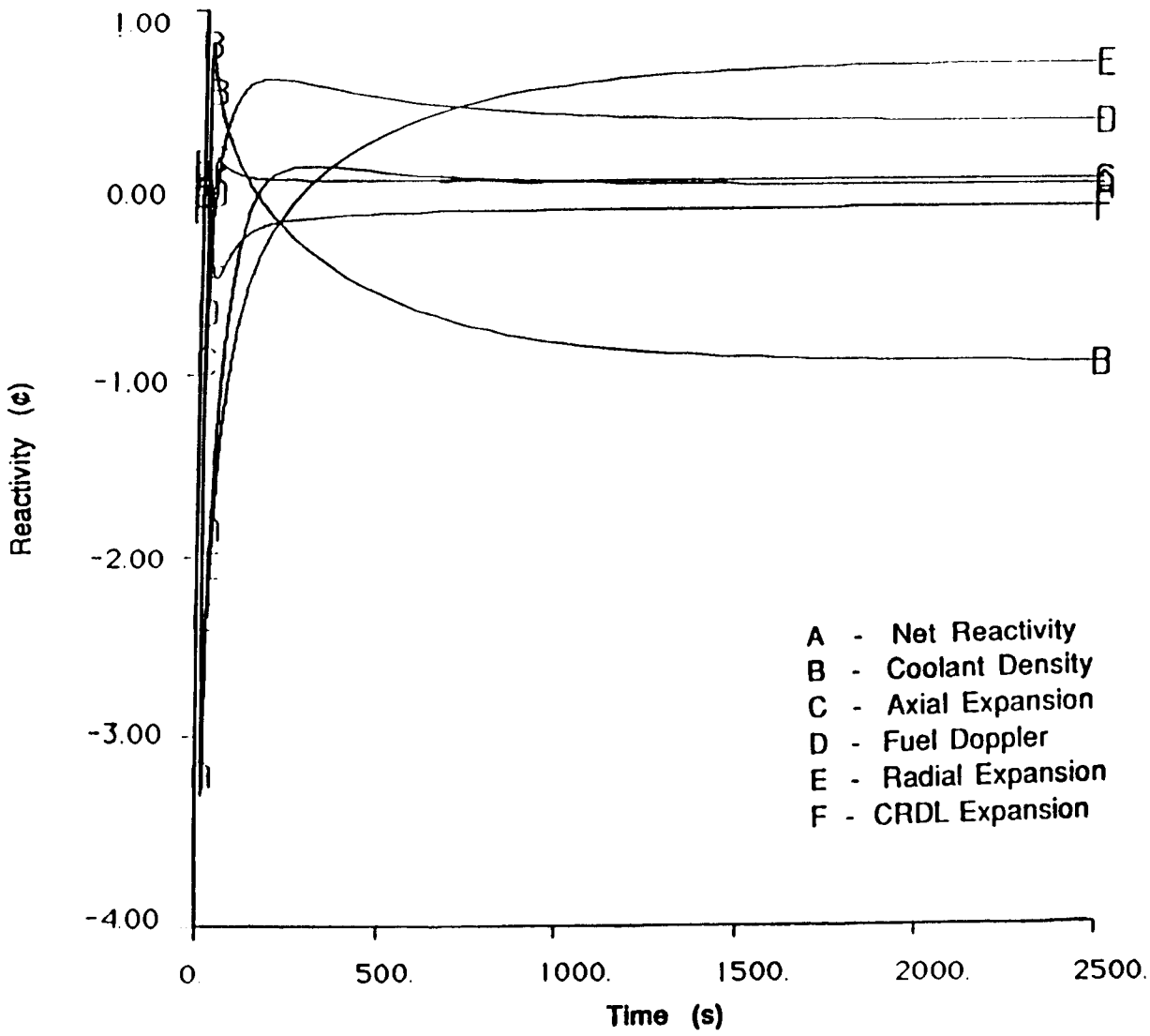

Figure 3.5 Long Term Reactivity Effects For 25% Step Reduction In Primary Pump Demand.

the primary loop cools and it approaches zero over the 2500 seconds of the transient as the reactor power reaches a steady state. Figure 3.6 shows the effect of the net reactivity and confirms the power behavior expected from the frequency analysis. The power rapidly drops to 90% and then slowly rises to almost 95% as the transient response settles and the reactivity effects reach equilibrium. It should be noted that during this transient, core outlet temperature remains several degrees higher than its original steady state, core inlet temperature decreases almost 20°F in the first 1000 seconds, and fuel temperature stabilizes several degrees lower than its original value. The drop in inlet and fuel temperatures, and the reactivity effects that result from this thermal behavior, cause the slow rise in power as the transient progresses.

The coolant density reactivity effect shows the expected prompt positive contribution ($0.008 giving a gain of -29.7 dB) with the subsequent transition to the in-phase (negative reactivity) behavior coming as the inlet coolant temperature drop yields a reduced average coolant temperature in the core after almost 200 seconds. The radial expansion/rod bowing reactivity, the fuel Doppler reactivity, and the fuel/cladding axial expansion reactivity provide the prompt negative effect indicated in their frequency response (-$0.028 ≈ -19 dB, -$0.007 ≈ -31.5 dB, and -$0.01 ≈ -27.8 dB, respectively). In addition, the steeper slopes of the radial and axial expansion reactivities, as shown in Figure 3.4, follow the expected gain behavior, with higher gains indicating greater rates of change. The coolant density and fuel Doppler slopes are similar, as are their gain in the frequency range between 0.1 and 1 rad/s. As the fuel temperature cools due to reduced heat production, the Doppler and axial expansion effects become positive, as suggested by their frequency response phase behavior, with the transition occurring after 20 to 30 seconds. Note the transition in the shape of the axial expansion contribution indicating the switch from expansion mode to contraction mode as described earlier.

The radial expansion effect becomes positive after almost 500 seconds due to the contraction of the lower support plate with lower inlet coolant temperature. This behavior supports the phase observations described previously. The CRDL expansion effect peaks 30 seconds into the transient (-$0.005 ≈ -34 dB) after a delay of five seconds. The gradual slope mirrors the low gain and the delay follows from the almost negligible response at high frequencies. The CRDL effect remains negative throughout the transient as the phase behavior suggested. The long term behavior shows the coolant density and CRDL effects counterbalancing the positive contribution of the Doppler, radial expansion, and axial expansion reactivities as was exhibited by the low frequency phase relations (using the contraction mode axial expansion phase response). In addition, the rank of the magnitudes of the reactivity components follows the previously described low

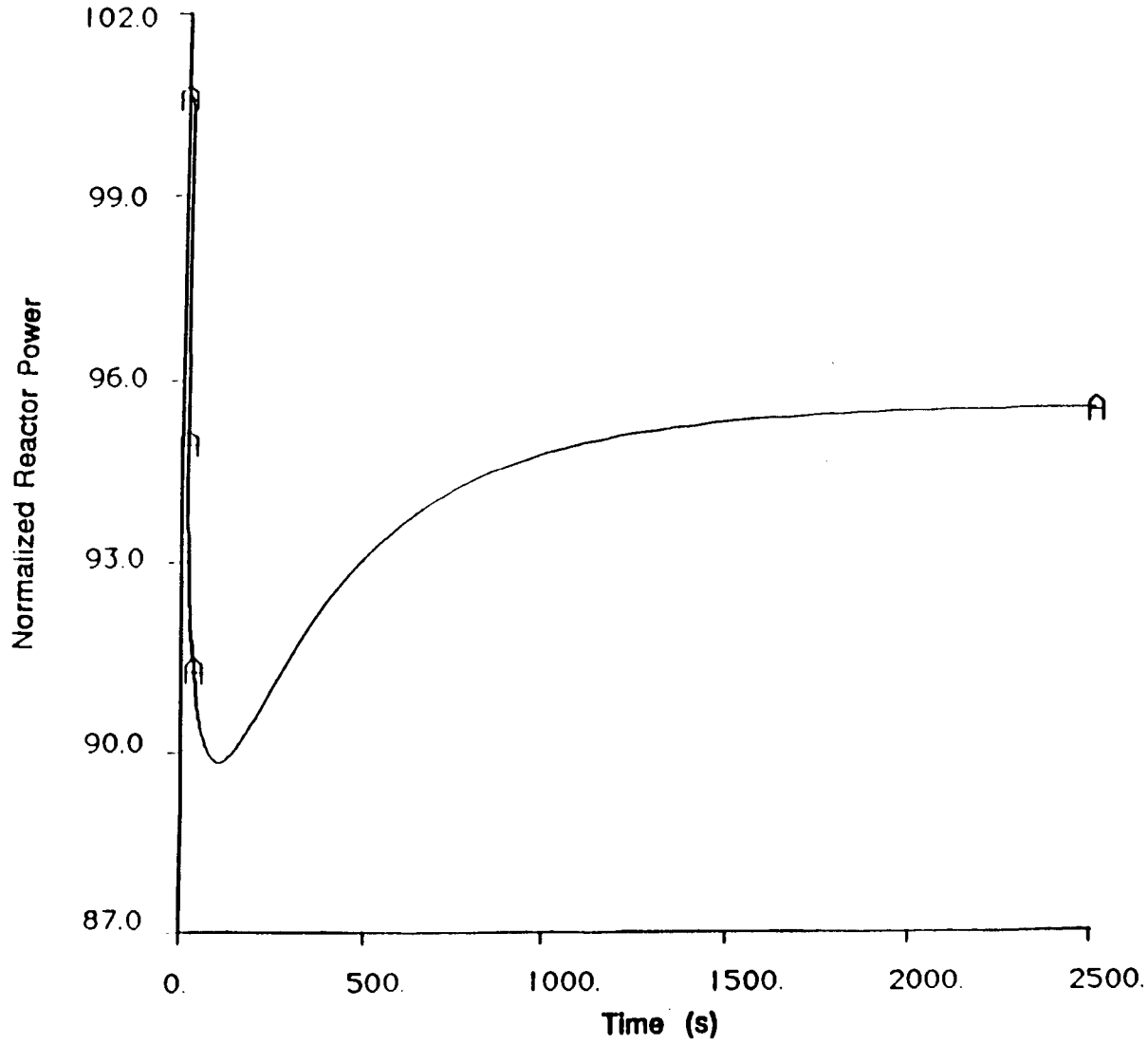

Figure 3.6 Reactor Power Transient Response For 25% Step Reduction In Primary Pump Demand.

frequency gains with coolant density providing a large negative effect followed by the positive contributions of radial expansion and Doppler broadening. Therefore, the dynamic response indicated by the frequency plots is supported by the time transient behavior of the model, indicating acceptability of the linear response results.

The observations drawn from the frequency response analysis as described, and supported by a time transient simulation, can be used to evaluate the inherent power control characteristics of the ALMR design. The inherent feedback dynamic response shows that controlling heat removal (heat removal = $Q \propto$ core flow * ΔT) can lead to inherent reactor power control as proposed. The whole-loop response observed in this analysis demonstrates the inherent stability of the reactor system. A change in heat removal leads to a prompt reactivity change, which changes heat production or power. As the transient continues, the altered heat production and removal effects feed through the coolant loops to cause adjustments in the thermal condition of the core (via higher outlet temperatures and lower inlet and fuel temperatures for a flow reduction) and bring the system to a steady state. Thus, the temperatures in the reactor system achieve a steady state, balancing production and removal by driving the reactivity feedback effects to equilibrium in the long term. However, the long term behavior of the open-loop model indicates that, for tight power control, the heat removal in the heat exchanger and steam generator need to be controlled in concert with core heat removal. For example, a gradual drop in the core inlet coolant temperature led to the beneficial transition of coolant density reactivity to a negative effect as the sample flow reduction transient progressed, but it also increased the positive effects of fuel Doppler and axial expansion by providing lower temperatures to drive the heat transfer and it instigated the positive radial expansion effect at around 500 seconds. By additional control of the coolant temperatures throughout the reactor system, it may be possible to guide the net reactivity to equilibrium more expediently, thus reducing the power recovery following the transient overshoot. Therefore, the behavior of loop temperatures must be evaluated along with the response of power to various candidates for controlling core heat removal to determine if inherent power control can meet the demands placed on the reactor during normal operation.

4.0 INHERENT REACTOR POWER CONTROL SYSTEM DESIGN

The dynamic performance of a plant system can be represented in either the time domain or the frequency domain. In contrast to other control studies of the SAFR plant, which dealt exclusively with the time response, this study determines the frequency response of the SAFR plant and uses that response as a design tool for a control system which utilizes the inherent feedback properties of the metal fuel design to accomplish load following control. The frequency response is presented as a set of Bode plots obtained from the MMS-SAFR model. Examples of Bode plots for a number of combinations of plant input and output parameters are presented. A physical interpretation of the features of the curves and an example of how these curves may be used in the design of a control system by classical control design methods are also presented. Finally, the tuning of that control system using a root locus approach to balance stability with controllability and the implementation and time transient evaluation of the control design are described.

Inherent reactor power control is really inherent neutron power control. Within some range, neutron power can follow the heat removal from the primary loop without being actively controlled by absorber rods. As demonstrated in Section 3, reactivity and power in the metal fuel core design have strong feedback characteristics associated with temperature changes. The frequency response plots of these feedback mechanisms show that they are sufficiently strong and responsive to consider inherent process stability as the control mechanism for reactor power. Because of its inherent stability, the plant could simply be controlled with the feedwater valve, at least over some small range of power and frequency. Open the valve and more power is transferred in the steam generator while holding all other controllable elements constant. However, even a small change in power would result in a large change in core temperatures, and the maximum rate of response would be quite slow. Yet, the idea does raise the question of how simple the control system can be and still meet specified performance requirements for load changes.

Aside from the control rods, there are four other active or controllable elements in the SAFR design: the feedwater flow, steam flow, primary flow, and intermediate flow.

The feedwater flow and steam flow are modeled as linearized valve equations. Both have the following general form:

$$W = k * W_{norm} * (\Delta P)/\Delta P_{norm} , \qquad (4\text{-}1)$$

where k is the normalized valve position,
W_{norm} is full flow,
ΔP is the pressure difference across the valve, and
ΔP_{norm} is the pressure difference at full flow.

In this simulation, the full flow pressure difference, ΔP_{norm}, for both the steam and feedwater valves is 50 psi.

The normalized valve position, k, is the controllable in this formulation. No valve dynamics are modeled. Therefore, the high frequency response of the flow to the valve demand is not attenuated by the response characteristics of an actuator.

The primary and intermediate pump/motor simulation includes modeling equations for the motor torque delay, rotational momentum, and fluid flow momentum. The controllable input to the pump/motor simulation is the motor torque demand. The dynamics of this model provide a realistic representation of the delay between the demand signal and the actual flow change.

For brevity, the terminology in this section usually refers to the controllables as feedwater, steam, intermediate, and primary flow. These names refer to the valve position or motor torque demand. The correct definitions are more precise from the point of view of the model but are less descriptive of the quantity being controlled.

The objective of this control design exercise is to design a simple control system for these four variables that gives acceptable load following performance from 40% to 100% power while utilizing the inherent feedback behavior to control reactor power. The MMS-SAFR plant model is a multi-input, multi-output system. The strategy for this control design exercise is to use a system of classical, proportional-integral, feedback controllers. The MMS-SAFR inputs and outputs are broken into individual control loops, each with a single-input, single-output relationship. The frequency response plots are used to select the input to output relationships and to set the preliminary gains. The features of the frequency response plots, such as corner or break frequency and phase crossover frequency, give the needed insight to select good input to output relationships for control. The control system gains are then refined using the root locus method to enhance system stability while maintaining controller performance.

Frequency response methods were chosen over more esoteric modern control techniques because of the simplicity of application and the insight into the underlying physical processes that this technique provides. It is an easy technique to apply and produces very credible control designs. In the future, the understanding obtained from the classical system design may lead to more elegant control designs that address specific problems while the classical

system response can be a benchmark by which new inherent power control system designs may be measured.

4.1 Load and Steam Pressure Controllers

The basic objective of the power plant control system is to make the power production follow the load demand. There are a number of possible combinations of controllables and observables by which load following could be achieved. The power of the plant can be measured in any number of places, for example, as neutron power, heat balances ($Q = W \cdot c_p \cdot \Delta T$) across the core, intermediate heat exchanger or the steam generator, or turbine/generator power. Also, each plant controllable affects each measure of power differently. Figures 4.1 and 4.2 show the frequency response of two measures of power at opposite ends of the plant to all the available controllables.

The units of the transfer function are the ratio of the observable and controllable units. The transfer function for power to rod worth is fraction of power per dollar of reactivity. The units of power to primary or intermediate flow are fraction of full power per fraction of full motor torque. For steam and feedwater flow, the transfer functions are in terms of fraction of full power per fraction of valve position.

The comparison of the power response at opposite ends of the plant to the same set of controllables illustrates dramatically the overriding factor in inherent power control. A control action near the reactor (e.g., control rods or primary flow) yields a steam generator power response that lags far behind. The response of the reactor power to steam or feedwater flow is similarly delayed. It is difficult to control power in this plant at either end and keep the whole plant moving in unison. Tables 4.1 and 4.2 list some data by which the responses can be compared. The data are obtained visually and are therefore approximate. Although the inherent power control scheme seeks to minimize or eliminate the use of rods, the frequency response to rod control is shown for comparison. As expected, the reactor power is most responsive to the rod motion input. Rod control offers a prompt power response, with a break frequency above 1 rad/s and essentially unity gain over almost the entire frequency range. The power response is in-phase with control rod reactivity for rates of change approaching 1% per second. The delay due to the control rod drive mechanism is the only dynamic limitation in the power response to rod motion. By comparison, no other controllable acts so quickly to change neutron power.

Of the candidates for inherent reactor power control, the transfer function of reactor power to primary sodium flow has the

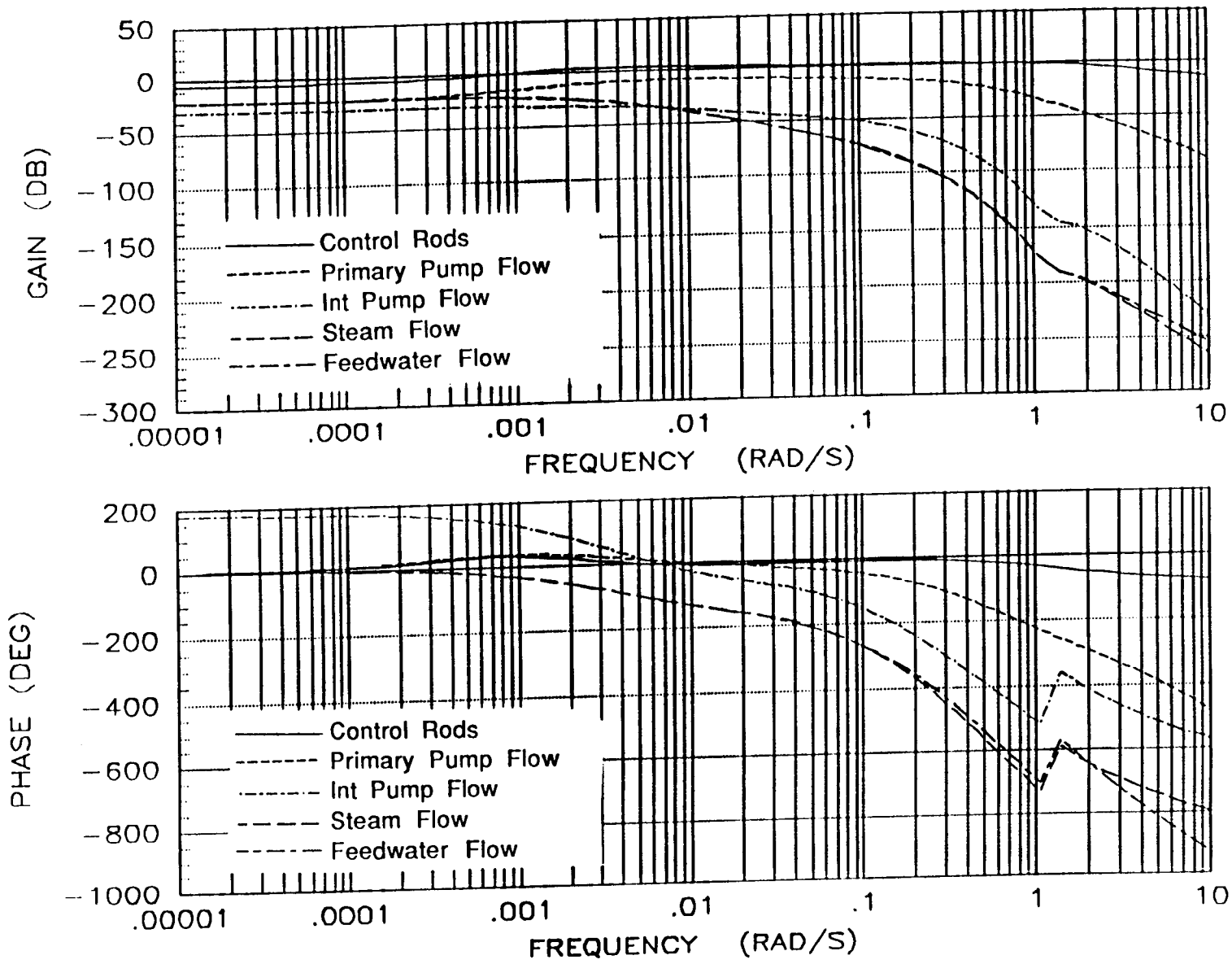

Figure 4.1 Frequency Response of Reactor Power to Each Controllable.

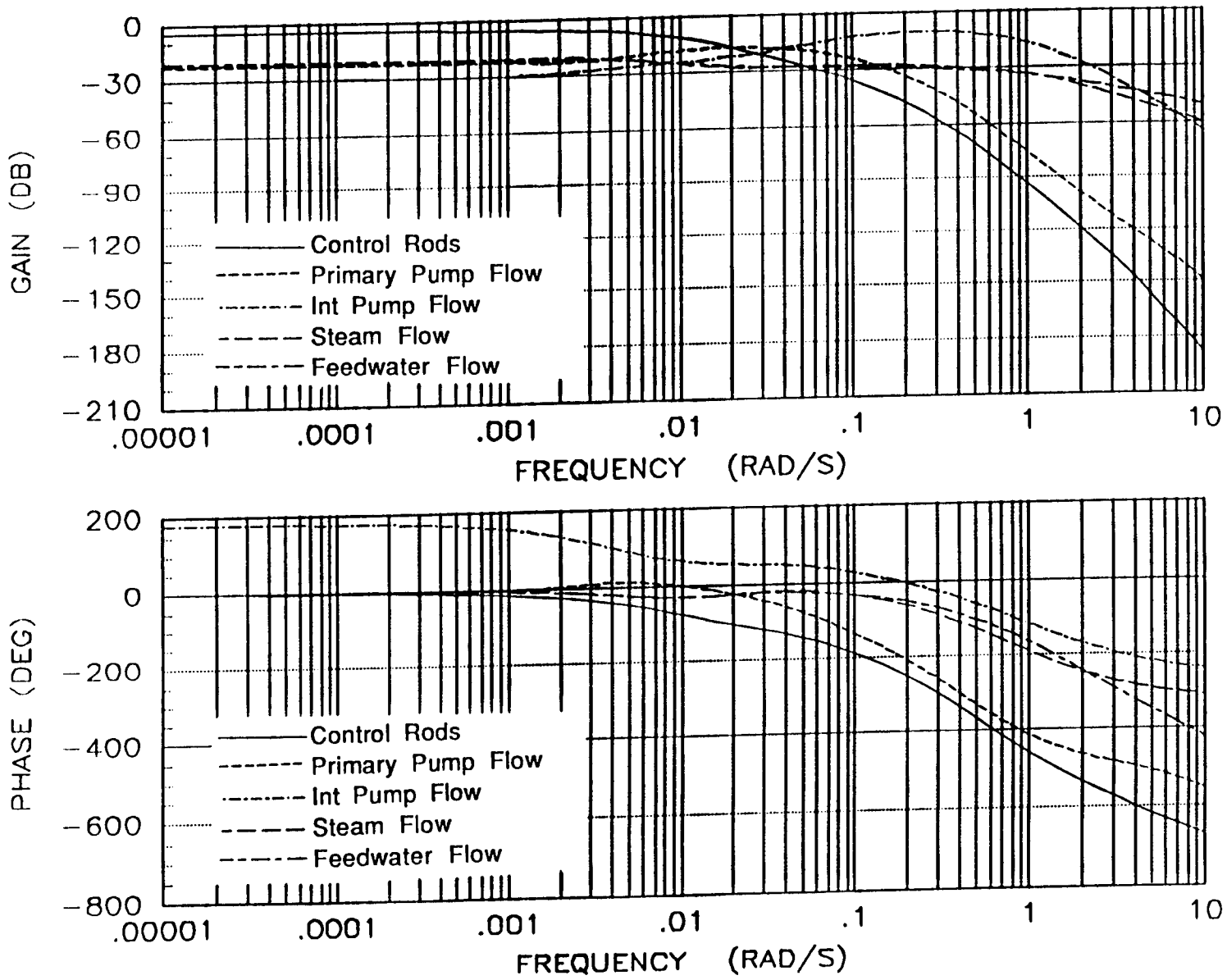

Figure 4.2 Frequency Response of SG Power to Each Controllable.

Table 4.1 Key Features of Transfer Functions of Reactor Power to All SAFR Controllables†

Controllable	Corner Freq	-180° Crossover Freq	Steady State Gain	Peak Gain	Peak Freq
Control Rods	1.0	>10.	0.316	3.16	0.0035
Primary Flow	0.32	0.65	0.09	0.1	0.006
Int Flow	0.003	0.12	0.0316	np*	np
Steam Flow	0.0035	0.0045	0.09	np	np
Feedwater	0.0035	0.0045	0.09	np	np

* np - No peaks

Table 4.2 Key Features of Transfer Functions of Steam Generator Power to All SAFR Controllables†

Controllable	Corner Freq	-180° Crossover Freq	Steady State Gain	Peak Gain	Peak Freq
Control Rods	0.006	>10.	0.316	np*	np
Primary Flow	nc**	nc	0.09	0.133	0.03
Int Flow	nc	nc	0.0316	0.1	0.3
Steam Flow	0.4	0.85	0.09	np	np
Feedwater Flow	0.6	1.1	0.09	np	np

* np - No peak
** nc - No corner

†Gains are in controllable per observable units while frequencies are rad/s.

highest corner frequency and phase crossover frequency, 0.42 rad/s and 0.63 rad/s. The primary flow response experiences a drop in gain at frequencies below roughly 0.03 rad/s. The decrease is due to cancellation effects that occur at low frequency where temperature effects have time to propagate completely around the loop. A similar but smaller drop is seen in the rod response at the same frequency. The same time constant is evident in the reactivity behaviors studied in Section 3, especially with the drop in gain of the net reactivity below this frequency. The time required for a lump or packet of sodium to completely traverse one pass through the coolant loop yields this loop circuit frequency.

The other controllables, intermediate, steam, and feedwater flow, all have much lower corner frequencies than rods or primary flow due to the time delay for propagating a temperature change from the steam generator or IHX to the core. The intermediate flow has the lowest steady state gain and goes to 180° out-of-phase at steady state. The responses due to steam and feedwater flow show almost identical behavior. The dynamic behavior of power for each of these three controllables exhibits a slight notch in gain at high frequency and a phase shift of 180° just above 1 rad/s. The frequency response gain at the notch is quite low. This behavior may correspond to a cancellation frequency due to the transit time within some component or region. It may also be a numerical aberration that occurs at very low gain.

Figure 4.2 shows the transfer functions for steam generator power to all controllables. The highest corner frequencies and phase crossover frequencies belong to the feedwater and steam flow controllables. The primary and intermediate flows both exhibit a mild resonance. The frequencies at the peaks correspond to the loop circuit frequencies of $2\pi/200 = 0.0314$ rad/s for the primary and $2\pi/20 = 0.314$ rad/s for the intermediate. The steam and feedwater exhibit a slight cancellation effect that is particularly evident at the primary loop frequency, 0.0314 rad/s.

In power maneuvering, it is important to match electrical generation to demand as well as possible. If a change in load demand were matched perfectly at the reactor using rod control, the change would show up 200 seconds later in the steam generator power. A delayed response of this magnitude is unsatisfactory for normal load control. The typical observable for load following is the generator power or megawatts electric. Since the MMS-SAFR model does not have a turbine model, the observable that is physically closest must be substituted. The best substitute for the load observable is then the steam generator power. The steam generator power is estimated by a heat balance across the sodium side of the steam generator.

The controllable for the steam generator load must now be selected. Good load following would be indicated by a high

corner frequency, a wide, flat low frequency response, a high gain, and a high frequency for the phase crossover in the transfer function of the steam generator power to controllable. As already noted, load following of the steam generator in response to control action at the reactor is very slow. The corner frequency for steam generator power with respect to rod reactivity is 0.006 rad/s. As one intuitively expects, the steam and feedwater flow controllables, which are closer to the steam generator, have a more direct effect on the steam generator power and thus have a wider bandwidth. Therefore, by quick inspection of the Bode plots, two obvious choices for the load controller emerge, load control based on steam generator power with either steam flow or feedwater flow as the controllable.

To focus on these two choices, the frequency responses of the steam generator power to feedwater flow and to steam flow are plotted again on a smaller scale for comparison in Figure 4.3. The responses are essentially identical, and, based on this information alone, load control could be performed by either. However, turbine control also requires a reasonably steady pressure at the throttle valve. The controllable <u>not</u> chosen for load control is likely to be chosen to control pressure. The choice becomes which of the two is better suited for use as a pressure controller. The responses of steam pressure to feedwater and steam flows are shown on Figure 4.4.

The pressure to feedwater flow gain has a very deep notch filter shape. The notch occurs at about 0.08 rad/s. Evidently, a strong cancellation or anti-resonance occurs at this frequency. A calculation of the transit time (mass divided by flow) for the steam/water side of steam generator gives value of approximately 88 seconds. This corresponds to a frequency of 0.07 rad/s. On an increase in feedwater flow, there are two competing processes which affect the steam pressure. First, the additional subcooled feedwater tends to have cooling and depressurizing effect. Second, increased flow yields additional mass in the boiling region, which increases the length of the region and, thus, the rate of steam production. Pressure increases when steam production increases. At the observed frequency, the two effects apparently cancel out, thus giving a very low gain for the transfer function.

The modeling of the boiling channel in the steam generator is an attempt to model all the dynamic processes that contribute to boiling instability. The model may or may not accurately reflect the true boiling stability. If the model is adequate, the once-through design is right on the edge of stability. At present, there is no other model or experimental data available for comparison. Very small modifications in the way the entering and exiting flow resistances are calculated by the steam and feedwater valve models can make the problem unstable for the open-

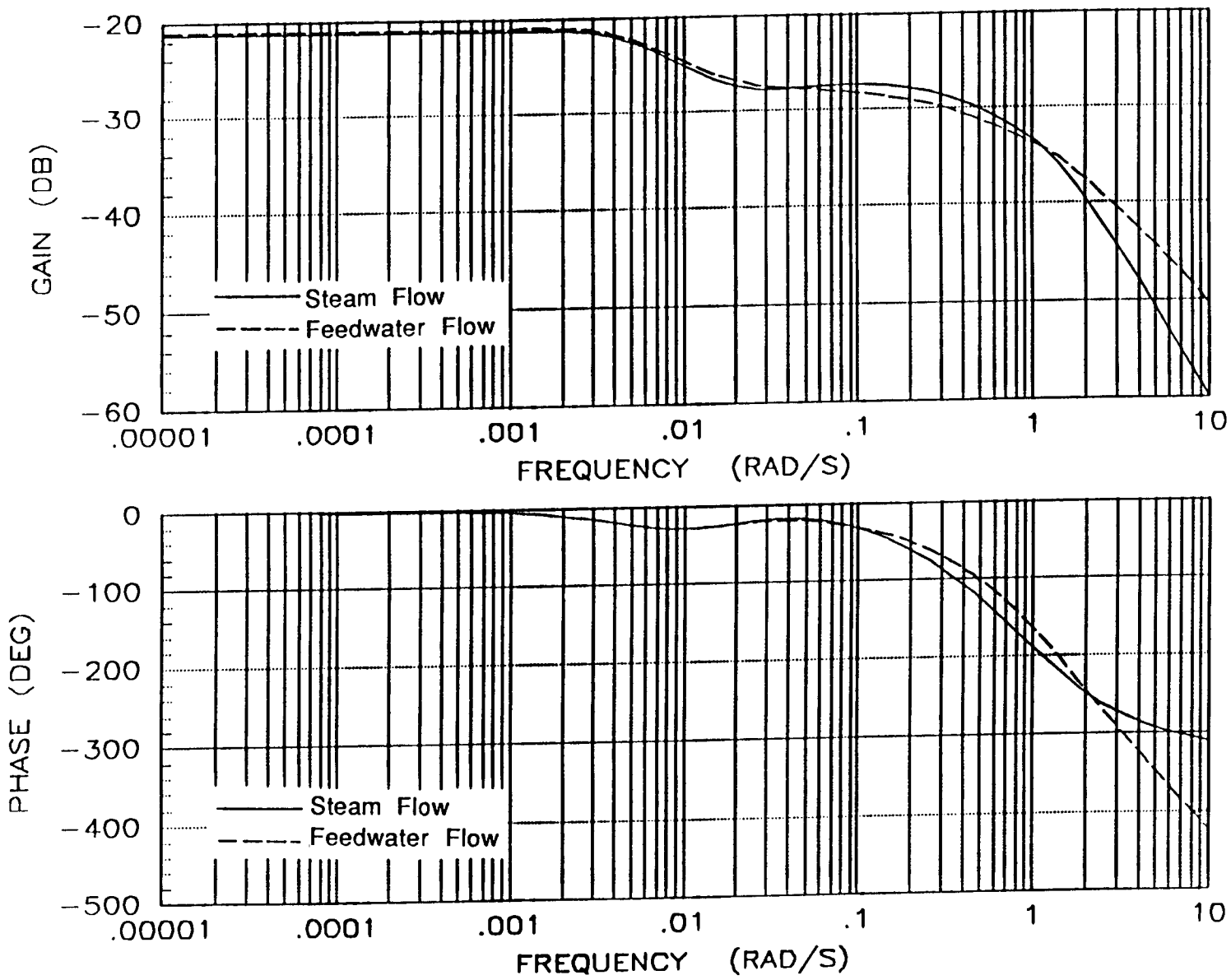

Figure 4.3 Frequency Response of SG Power to Steam & Feedwater Flows.

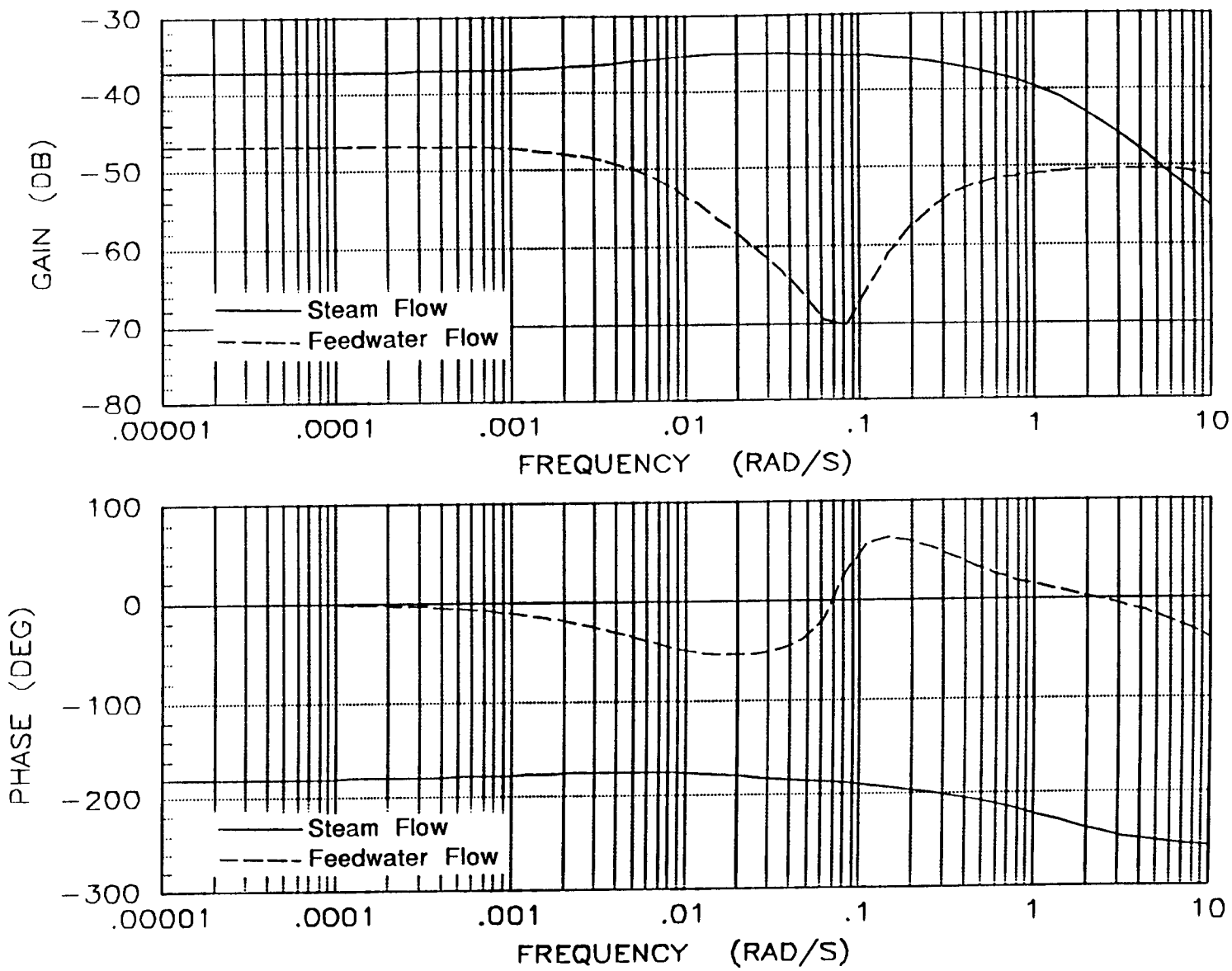

Figure 4.4 Frequency Response of SG Pressure to Steam & Feedwater Flows.

loop response. Some consideration of the stability margin requirements should be performed on this boiler design.

Regardless of the process dynamics leading to the shape of the steam pressure to feedwater flow frequency response, this observable/controllable pair does not have the wide, flat gain that makes controller design easy. Compensating for such a notch is possible but requires a clear knowledge of the cause of the notch and accurate calculation of its location and extent. Thus, feedwater flow appears to be a poor choice for controlling steam pressure. A preliminary transient calculation using feedwater to control steam pressure confirmed this indication.

The other frequency plots show some features at the loop frequencies for primary or intermediate flow, but none exhibit a large resonance or cancellation as in the pressure to feedwater flow response. Based on the frequency plots, steam flow is the obvious choice between the two possibilities for pressure control, and feedwater flow is the choice for steam power control. This conclusion is far more apparent from the frequency response plot than from either an intuitive understanding of process physics or time response transients.

The open-loop frequency response can now be used to select preliminary controller parameters. The open-loop frequency response of each observable/controllable pair is affected by the other control loops. Consequently, it is not possible to calculate the gains from the open-loop transfer function perfectly. The gains selected using the open-loop transfer function are typically the maximum, safe values assuming no other active control elements in the system. Frequently, when several controllers are combined, the net system response is not satisfactory. Lower gains may be selected by plotting a root locus to improve the system stability.

One common rule of thumb for obtaining a suitable gain is to set the controller gain such that the combination of the process open-loop gain and controller gain gives a phase shift of -135° at the point of unity gain. The frequency at which this occurs is called the gain crossover frequency. Using this number as the feedback gain gives a closed-loop response with a 45° phase margin in the closed-loop system. As shown in graphically in Figure 4.5, the -135° phase shift occurs at 0.79 rad/s, which corresponds to -32.5 dB gain for the steam generator power to feedwater flow transfer function. Converting the proportional gain to its conventional units yields a value of 42 with units of fraction of valve position per fraction of load.

The integral portion of the controller introduces a pole in the closed-loop response. The pole should be placed such that it does not have much effect on the crossover frequency. Placing the pole at least one decade in frequency lower than the

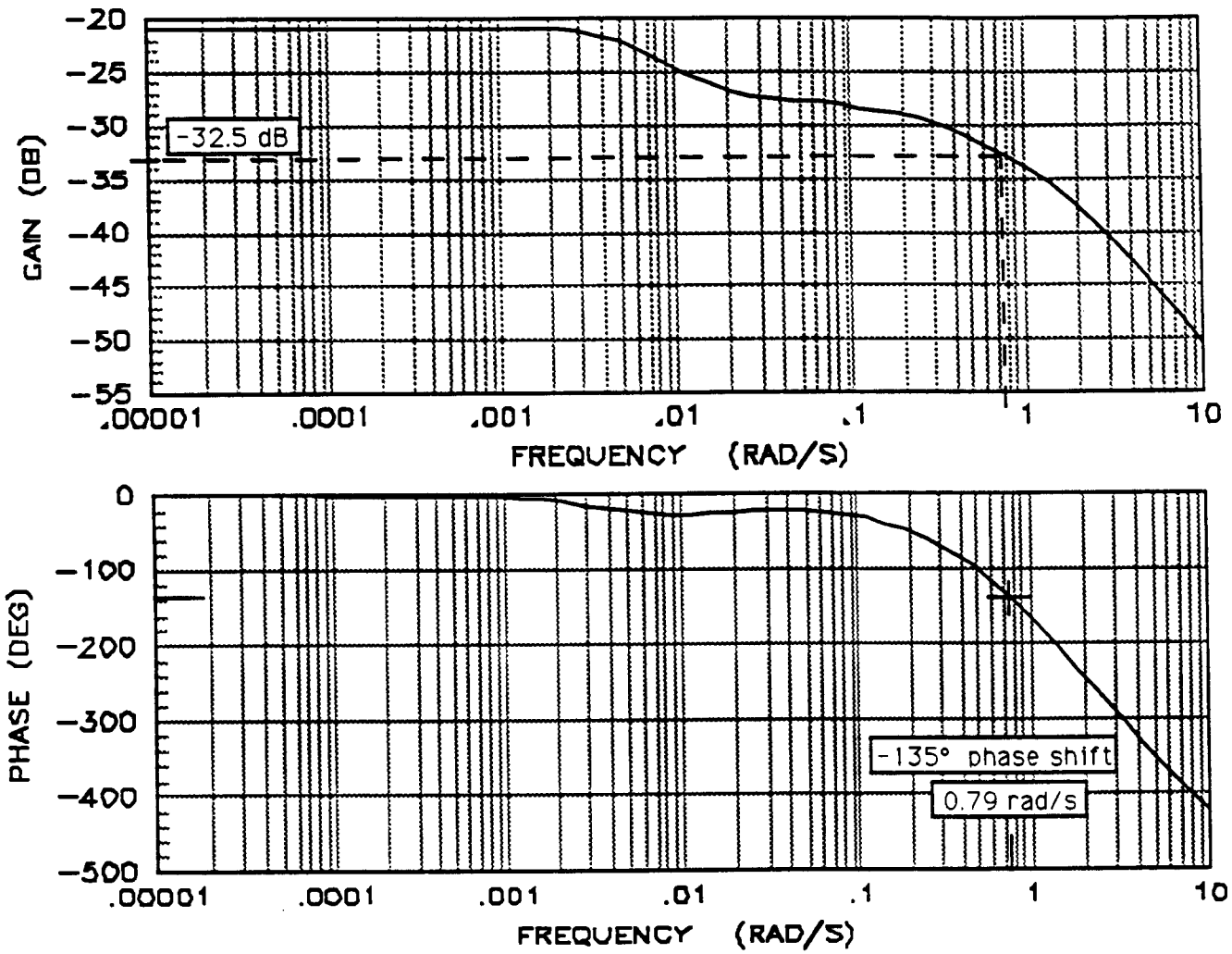

Figure 4.5 Graphical Determination of Gain Compensation and Reset Rate for Feedwater Flow Controller.

crossover frequency changes that frequency less than 6%. Thus, a reset rate of 0.079 repeats per second may be safely chosen for the integral portion of the load controller.

The same procedure to estimate gains can be applied to the pressure control using steam flow. Except for the slight peak at 0.03 rad/s, the frequency response of steam pressure to steam flow has the approximate shape of a first order lag. At high frequency, the gain decreases 20 dB per decade and the maximum phase shift is 90°. Any gain could be chosen for this frequency response based on gsin compensation techniques. However, this frequency response is somewhat unrealistic at high frequencies because the model neglects the dynamics of the actuators and sensors. If a pole is placed at 1 rad/s to represent valve dynamics, then the phase shift passes through -135° at about this frequency. Calculating a gain at this point gives a value of 100 in terms of fraction of valve position per fraction of pressure drop. The reset rate is (1 rad/s)/10 or 0.1 repeats per second.

4.2 Core ΔT Controller

There are two remaining control loops to define for the plant. They involve the controllables for the primary and intermediate sodium flow. First, consider the control loop involving primary flow.

The primary flow has been shown to be a strong reactor power or reactivity controller due to the inherent feedback effects. However, plant power is already being controlled by feedwater flow. A second controller on system power would result in a competing control because the two would never be perfectly matched at the same load setpoint. Thus, primary flow should not be used to control reactor power directly. Reactivity cannot be used easily because it is not a directly measurable quantity. Moreover, one does not really want to control reactivity to a setpoint. A better choice for the quantity controlled by the primary flow is one which enhances the inherent stability of the core and minimizes the thermal transients in the primary circuit.

One simple alternative is to hold flow constant. A quick mental experiment involving a load increase transient at constant flow reveals the following conclusions about the steady state temperature changes. The core temperature difference must increase to carry the increased power from the core, and the average core temperature must drop to generate the neutron power through negative temperature reactivity feedback. The increase in core temperature difference leads to an increase in outlet coolant temperature. As we have seen in Section 3, the prompt reactivity effects depending on outlet temperature (coolant, fuel Doppler, axial expansion, and control rod driveline expansion)

are negative as a whole, which is counter to the desired power increase. To achieve a power increase at constant flow, all the positive reactivity must come from decreasing the inlet sodium temperature. The inlet temperature change must be fairly large to compensate for the negative reactivity effects of both the power increase and outlet temperature increase. Also, from loop transit time considerations, the inlet temperature changes occur slowly. Therefore, constant flow seems a poor choice.

Another alternative is a flow setpoint program in which the setpoint depends on power. This scheme would use load demand as a feed-forward signal and offers a remedy to the problem of constant flow. Both inlet and outlet temperature could be made to decrease with increasing power demand by increasing the primary flow. The steady state decreases in inlet and outlet coolant temperatures per increase in power are approximately equal for a flow program that is proportional to power. This scheme causes the reactivity changes due to outlet and inlet temperature effects to act in the same direction and gives an approximation to the constraint for minimum RMS coolant temperature change. However, feeding the load demand straight into the primary pump demand changes the primary flow too soon and results in large sodium temperature swings. Preliminary simulations using the feed-forward scheme demonstrated this behavior. Filtering the feed-forward signal to minimize the temperature swings is possible but seems far too complex. A more direct approach is to use the pump flow to control the core temperature difference rather than the power. To illustrate the point, Figure 4.6 plots the frequency responses of various temperatures in the core to primary flow. The transfer function for core temperature difference to primary flow gives the characteristic shape of a good observable/controllable pair. It has the high frequency response characteristics similar to that gained by controlling outlet temperature with flow and the low frequency response behavior obtained by controlling inlet temperature using primary flow. The temperature difference observable is a clear pick over any single temperature that might be chosen.

The gains can be calculated graphically at the -135° phase shift frequency, which occurs at 0.42 rad/s. A proportional gain of 0.022 fraction of motor demand per °F and a reset rate of 0.042 repeats per second are calculated from the plot.

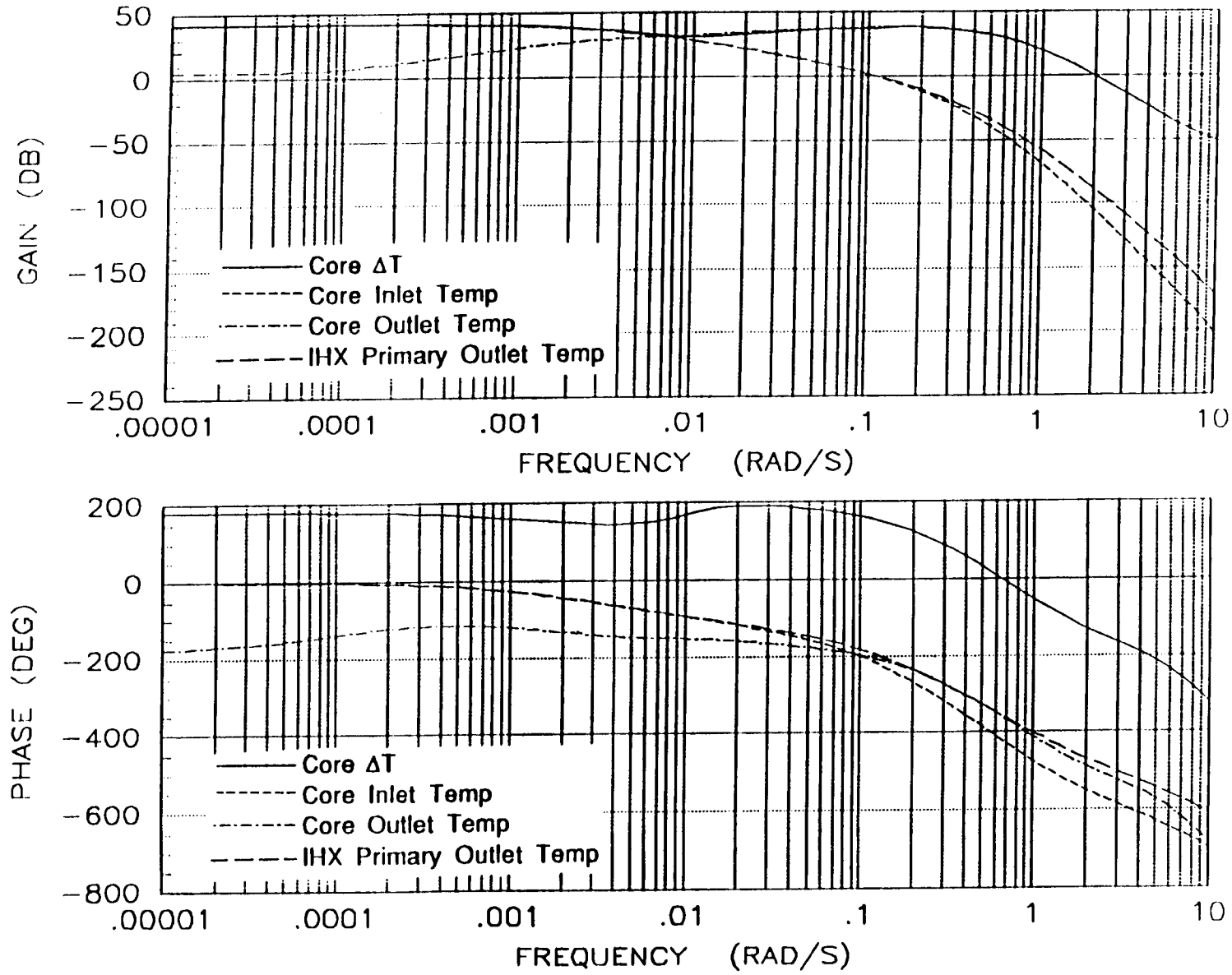

Figure 4.6 Frequency Response of Primary Loop Temperatures to Primary Flow.

4.3 Intermediate Loop Temperature Controller

The controllers selected to this point have not fixed an absolute temperature. The feedwater and steam flows control load and steam pressure, respectively. The primary flow controls core temperature difference. The last remaining controllable, intermediate loop flow, should be used to control temperature in the intermediate loop to minimize temperature transients there. Let us consider what temperature variable can best be selected. The likely candidates are the IHX intermediate outlet temperature, the IHX primary outlet temperature, the SG intermediate outlet temperature, or steam temperature. One might also consider controlling a primary loop sodium temperature to limit thermal transients there. As the results of this section demonstrate, the primary sodium temperatures must be free so that inherent stability can control neutron power. Thus, controlling a primary temperature is not a good choice. The steam temperature is possible, but time delays in the heat transfer process between the intermediate and water sides of the steam generator make steam temperature a poor choice.

Frequency plots of the potential observables to intermediate flow response functions, shown in Figure 4.7, give a basis for selecting a temperature to control using the intermediate flow. The primary question is how well each temperature responds to changes in intermediate flow. To help illustrate the problem with controlling a primary sodium temperature, the linearized system model used to obtain these frequency plots has the previously designed controllers for load, steam pressure, and core temperature difference active. The gain plot shows the two intermediate sodium temperatures and steam temperature grouped together. The primary sodium temperatures are also grouped together. These temperatures respond as pure derivatives below 0.005 rad/s. The derivative shape is an indication that the primary sodium temperatures cannot be controlled with the intermediate flow as their behavior is determined by other effects. The inherent stability mechanism of the core controls reactor power through temperature feedback. With the core temperature difference and load controllers active, there is only a single reactor inlet or outlet temperature that matches both load demand and the temperature difference demand at steady state. To have a steady state, the intermediate flow controller would have to control primary temperature to exactly that point. Since the unique temperature which satisfies load and temperature conditions cannot be known precisely at all times in core life for all power levels, the primary temperatures cannot be controlled by intermediate flow given the control design decisions already made. This insight into the plant process could be seen in other ways, but the derivative behavior illustrated by the frequency plot indicates the problem very quickly.

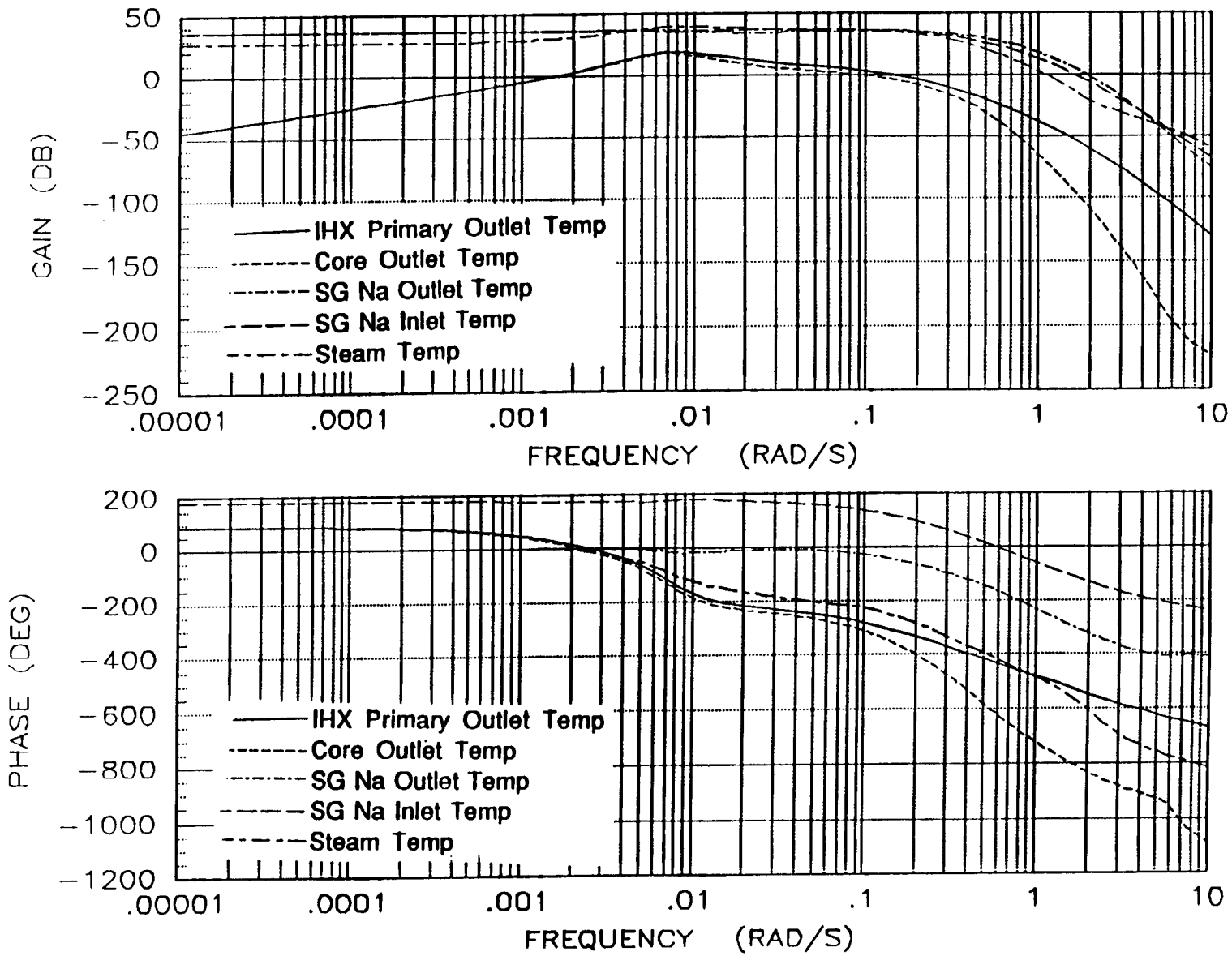

Figure 4.7 Frequency Response of System Temperatures to Intermediate Flow (Note: other controllers are active).

Judging from the frequency response plots, the outlet sodium temperatures from the intermediate side of the IHX and the steam generator and the outlet steam temperature of the steam generator are all reasonable candidates for control. The low value for the phase crossover frequency for the steam temperature makes it a poor choice. Of the other two possibilities, the exit temperature on the intermediate side of the steam generator is a slightly better choice because of its higher corner frequency.

For the steam generator outlet sodium temperature controller, the -135° open-loop phase shift frequency at unity gain occurs at 0.45 rad/s with a proportional gain of 30 dB or 0.0316 fraction of motor demand per °F. The reset rate is 0.045 repeats per second.

4.4 Root Locus Analysis

Evaluating the closed-loop system roots with the preliminary gains chosen from the Bode analysis shows the system to be unstable, having a pair of complex poles at (+0.317,+/-0.780). This result indicates that the preliminary gains are too high by a considerable amount. Reducing any of the system gains has some beneficial effect on the unstable poles. In this design evolution, the feedwater and steam controller proportional gains were reduced by a factor of 10 to shift the unstable pole to the stable region. Root loci were generated by individually varying the proportional gains for each controller downward from the open-loop starting point. Figures 4.8A through 4.8D show the loci of particular poles having the largest change for variations in each controller gain. It should be pointed out that the pole pair that originally showed up as unstable were actually more sensitive to the intermediate flow gain than to the gains for feedwater and steam flow. The range of gains shown is represents one decade of change in the controller proportional band. The reset rates are held constant.

The loci for the steam and feedwater flows are increasingly stable for increasing gain. The steam flow lies on the real axis, and the feedwater flow parallels the real axis for large gain. This means that the controlled variables, steam pressure and load, can be made as stable and responsive as desired by increasing the gain. This is a physically unrealistic situation and is due to neglecting the sensor and actuator dynamics. Also, increasing these gains tends to make other poles less stable. The final gains for the steam and feedwater are chosen so that the poles are reasonable in magnitude and lie closer to the origin than the expected poles for the actuators. This provides a conservative approach to selecting gains and accounts for some of the approximations in the model.

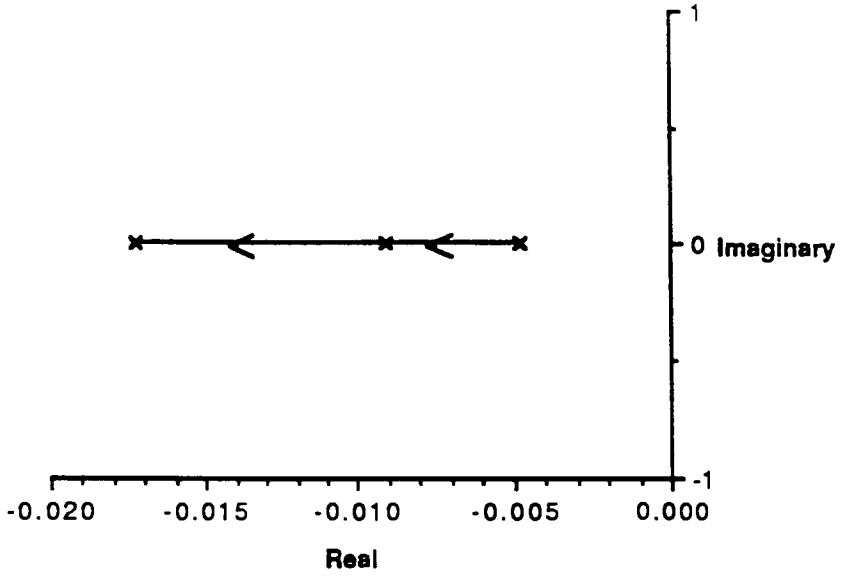

Figure 4.8A Steam Valve Controller Root Locus.

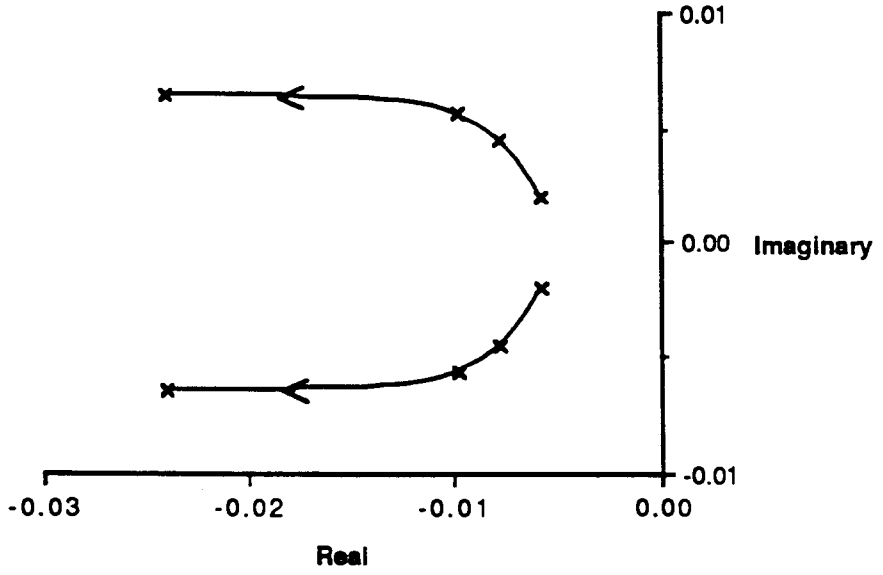

Figure 4.8B Feedwater Flow Controller Root Locus.

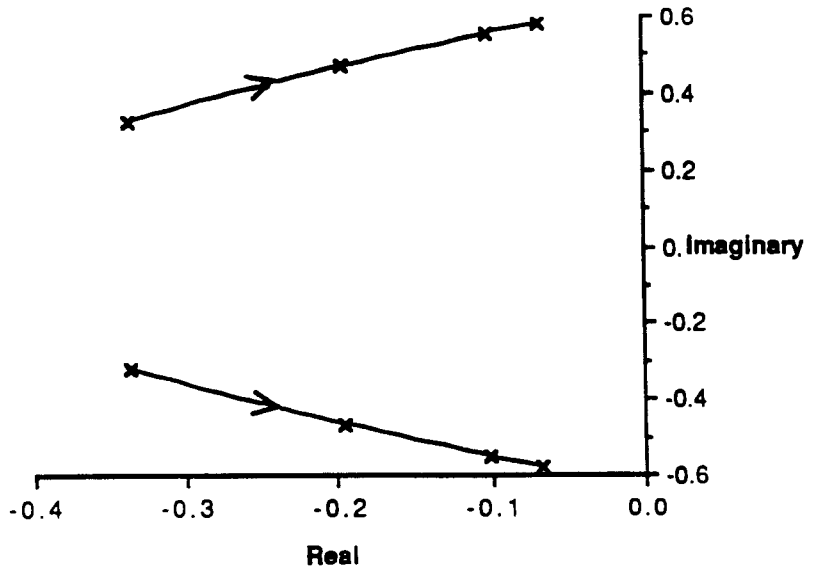

Figure 4.8C Intermediate Loop Flow Controller Root Locus.

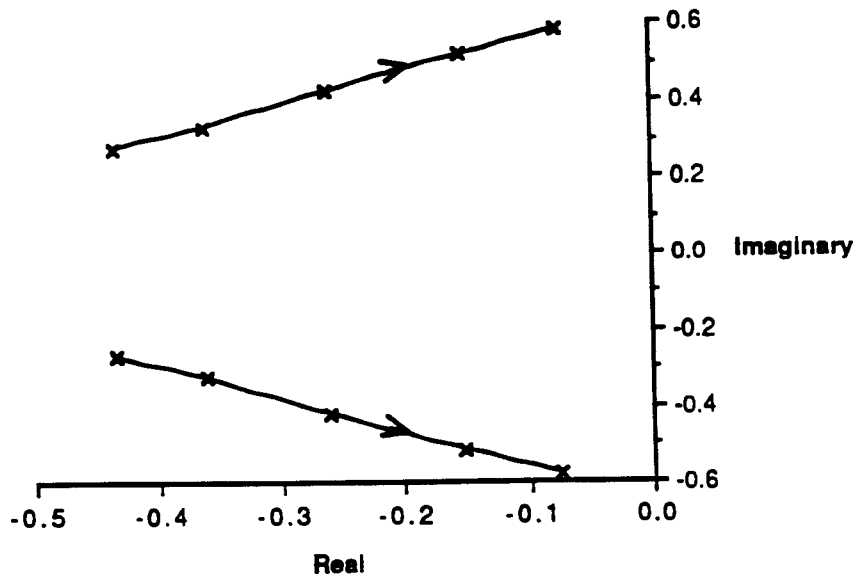

Figure 4.8D Primary Loop Flow Controller Root Locus.

The loci for the primary and intermediate flow controllers show decreasing stability as gain increases. The design objective for selecting final gains for the primary and intermediate flow is to select as the maximum gains possible without sacrificing stability margin. Selecting a gain at the intersection of the root locus and a line that makes a 45° angle with the negative real axis gives a damping ratio of 0.5. This point gives a reasonable compromise between response and stability.

The controller design is summarized in Table 4.3. This table lists the observable/controllable pairs and preliminary controller gains that were selected by the Bode frequency response methods. The final gains selected by root locus methods are also listed. Reset rates in the final settings were rounded slightly for convenience during the tuning procedure.

4.5 Closed-loop Performance

In this section, the closed-loop response of the system is presented in both the frequency and time domains. The frequency response is presented first. Evaluations of the closed-loop performance in the frequency and time domains are normally used to demonstrate that a controls design meets the performance requirements. The only controls-related performance requirements for the SAFR design are the normal operating range design requirements. These requirements [7] state that the reactor in normal operation must be able to follow load changes at a rate of 3% per minute without exceeding allowable temperatures in the fuel (2200°F), clad (1350°F), structure (1050°F), and coolant (1650°F). There are no explicitly defined controls design performance requirements for either the frequency domain, such as requirements for stability margin or cutoff frequency, or for time domain response, such as the response to a unit step in terms of rise time or overshoot. These quantities are presented in this section, but lacking a rigorous criterion, the acceptability of the design cannot be fully evaluated. The performance obtained from this test would seem satisfactory for most normal operating circumstances.

The closed-loop frequency response is created differently than that for the open-loop system. The closed-loop frequency response uses the setpoint as the controllable and the controlled variable as the observable. For example, the closed-loop transfer function for the feedwater controller is determined by

Table 4.3 Control System Design Summary

		Controller Settings*			
		Preliminary		Final	
Controllable	Observable	Prop Gain	Reset Rate	Prop Gain	Reset Rate
FW Flow	SG Power	100.0	0.1	4.0	0.1
Steam Flow	Steam Press.	42.0	0.079	2.5	0.1
Primary Flow	Core ΔT	0.022	0.042	0.005	0.04
Int. Flow	SG Sodium Outlet Temp	0.0316	0.045	0.01	0.05

*Gains are in terms of controllable per observable units while reset rates are in repeats/second.

the steam generator power to load demand frequency response. If the controller is well designed, then the low frequency gain is 0 dB and the response has a wide, flat gain with a sufficiently high corner frequency to meet the maneuvering requirements of the plant. Corners or peaks correspond to the dominant poles in the dynamic system. Figure 4.9 shows the frequency response of both the steam generator power and the reactor power to load demand. The corner or cutoff frequency for the steam generator power to load demand response is 0.5 rad/s. The reactor power cutoff frequency is 0.008 rad/s. The steam generator has a second, smaller corner at the same point. The system poles associated with each controller can be converted to frequencies and damping ratios. The pole associated in the root locus with the load controller gives a frequency of 0.00732 rad/s and damping ratio of 0.441. This pole corresponds to the lower corner in the frequency plot. The complex pole pair does not result in a large peak because of the relatively high damping ratio. Frequency and damping ratios of (0.477,0.571) and (0.496,0.496) result from the complex poles for the primary and intermediate flow controllers, respectively. The combined effect of these poles produces the upper corner frequency in Figure 4.9. The resultant peaks are indistinguishable in the gain plot. The existence of two complex pairs occurring at close frequencies is evident, however, in the phase plot, which shows a total phase shift of 360°. The lower pole pair, resulting from the primary flow behavior,

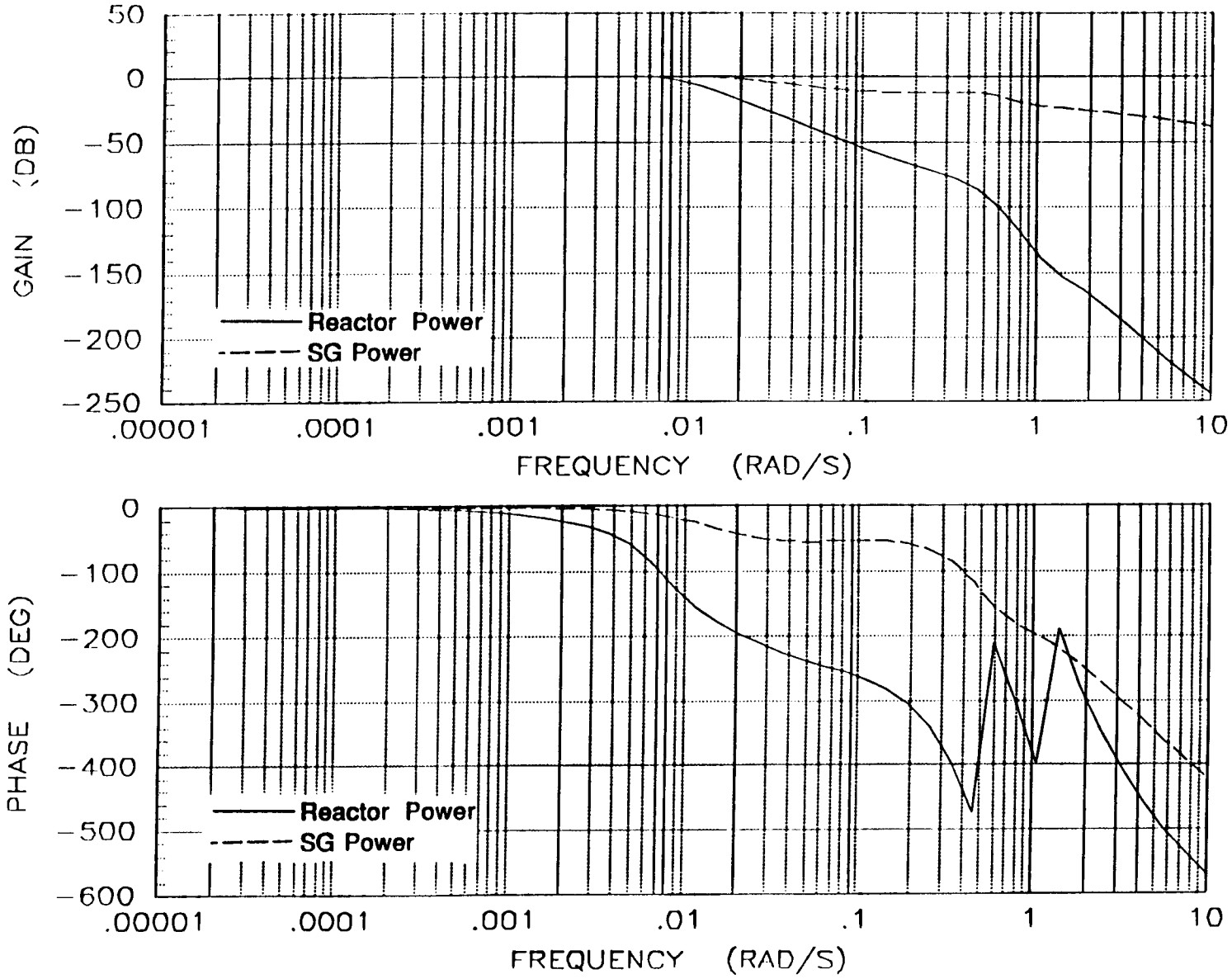

Figure 4.9 Closed-Loop Frequency Response of Reactor Power & SG Power to Power Demand.

characterizes the reactor system response to a step change in load. The upper pole pair, derived from the intermediate flow controller, characterizes the steam generator response. The frequency responses for steam generator power and reactor power show that the control system has reasonable stability and rate of response. From this plot, acceptable transient response would be expected.

The final test of the control design exercise is a closed-loop time simulation to evaluate the maneuvering performance of the control system in the time domain and to test the assumptions made in the control design, such as model linearization. The chosen transient is a 10% step change in load demand. The simulation uses the nonlinear, MMS-SAFR model and the controllers designed herein. The time transient is used to evaluate standard performance criteria, such as rise time, settling time, overshoot, and steady state error. The rate of response is also calculated. Since the simulation uses the the full nonlinear model of the plant, the transient simulation can be used to test that the response remains stable as the plant moves away from the point of linearization. The results are shown in Figures 4.10A through 4.10H.

The power response in Figure 4.10A shows smooth continuous change. The steam generator power drops quickly to the load demand point followed by a mild overshoot and smooth, damped settling at the new load demand point. The rise time or point at which the response is 90% of the input step is 35 seconds. The settling time or point at which the response reaches and remains within 1% of the setpoint is 200 seconds. The steady state error is zero. The overshoot is 0.3% of full power. Over the first several seconds of the transient, the steam generator response is a linear ramp with rate of change of 17% power per minute. This rate of change indicates that the steam generator would be able to follow a 3% per minute ramp in demand easily, as specified in the design requirements for normal load changes. The reactor power in the same figure also has a smooth damped behavior, but it responds much more slowly. The performance parameters for the reactor power are rise time, 225 seconds; settling time, 1200 seconds; overshoot, 1.5%; and ramp rate of 2.7% per minute. There is no steady state error. The steady state difference between the reactor power and steam generator power is due to a normalization factor for reactor power that does not account for the pump power precisely.

There is a large transient difference between heat production and heat removal during this simulation. The difference results from the amount of energy required to raise the primary sodium pool temperatures to initiate the reactivity feedback effects. The plot illustrates again the delay between primary and steam generator effects. From the standpoint of core safety, the delayed response at the reactor is desirable because

it prevents a rapid temperature rise in the core due to upsets in the balance of the plant. However, large delays may present a problem to the controls designer. The delays in the system can determine the stability limits. The control design presented here does not push the system too fast so the response is stable. As seen in the root locus analysis of Section 4.3, instability results if faster response is attempted through simply raising the control system gains. This is the disadvantage presented by the delay between primary and steam generator power response. If the level of performance seen here is satisfactory, then inherent reactor power control with proportional-integral controls can be used. If faster reactor power control is desired to meet more severe duty cycle requirements, additional control through a more direct control mechanism, such as control rods, is required. More sophisticated control design techniques, such as multivariate optimal control, could probably be used to achieve faster response.

The system temperatures are shown in Figures 4.10B through 4.10E. Maximum temperatures are well within the operational limits. The 10% step change would not normally be expected to approach any of these limits. Inherent reactor power control does raise the mixed average coolant temperature at the reactor outlet from 950 to 959°F as power decreases from 100% to 90%. If the correlation is perfectly linear, the coolant temperature at the lower limit of automatic operating range of 40% power would be 1004 °F. The structural temperatures in the hot pool are close to this temperature. At low power, this inherent reactor power control scheme does not leave much operating margin for the structural temperature of 1050 °F. The controlled temperatures, core ΔT and steam generator outlet sodium temperature, are both well controlled. The pump flow controllers are apparently performing well based on Figures 4.10D and 4.10E.

The primary and intermediate loop flows are shown in Figure 4.10F. Since the core ΔT control works very well, the primary flow response is very similar to the reactor power response. Interestingly, both intermediate and primary flow change more than 10% for the 10% load change. This is an indication that a load dependent setpoint for the intermediate loop temperature may be necessary to accomplish a load swing from 100% to 40% power.

The steam generator flows and pressure are shown in Figures 4.10G and 4.10H. The long term response of these variables is well behaved. In the short term, there are spikes in pressure and flow. The question of boiling channel stability arose in the frequency analysis of the pressure to feedwater flow response. Although the control system cannot solve the problem of boiling instability, the model used in this analysis does attempt to represent the phenomenon. Since boiling stability decreases with decreasing load, there is concern that the boiling channel might become unstable at reduced load. The spikes on pressure and flow

are oscillations that indicate the presence of damped oscillator equations in the model of the boiling channel that are excited by the sharp change in feedwater flow. The oscillatory frequency is quite high and the oscillations are well-damped. This model indicates satisfactory boiling channel stability at 90% load. Additional analysis and testing at lower power is required to evaluate this concern fully.

Overall, the transient performance of the inherent reactor power control design developed for this work demonstrates the ability of the controller to handle potential load following maneuvers. As was expected from the root locus analysis, the controlled system is well behaved and responds with reasonable speed to a fast demand change. Most load manuevers will evolve on a slower time scale and the inherent reactor power control design should easily follow these events, satisfying the 3% per minute rate of power change specified for such events.

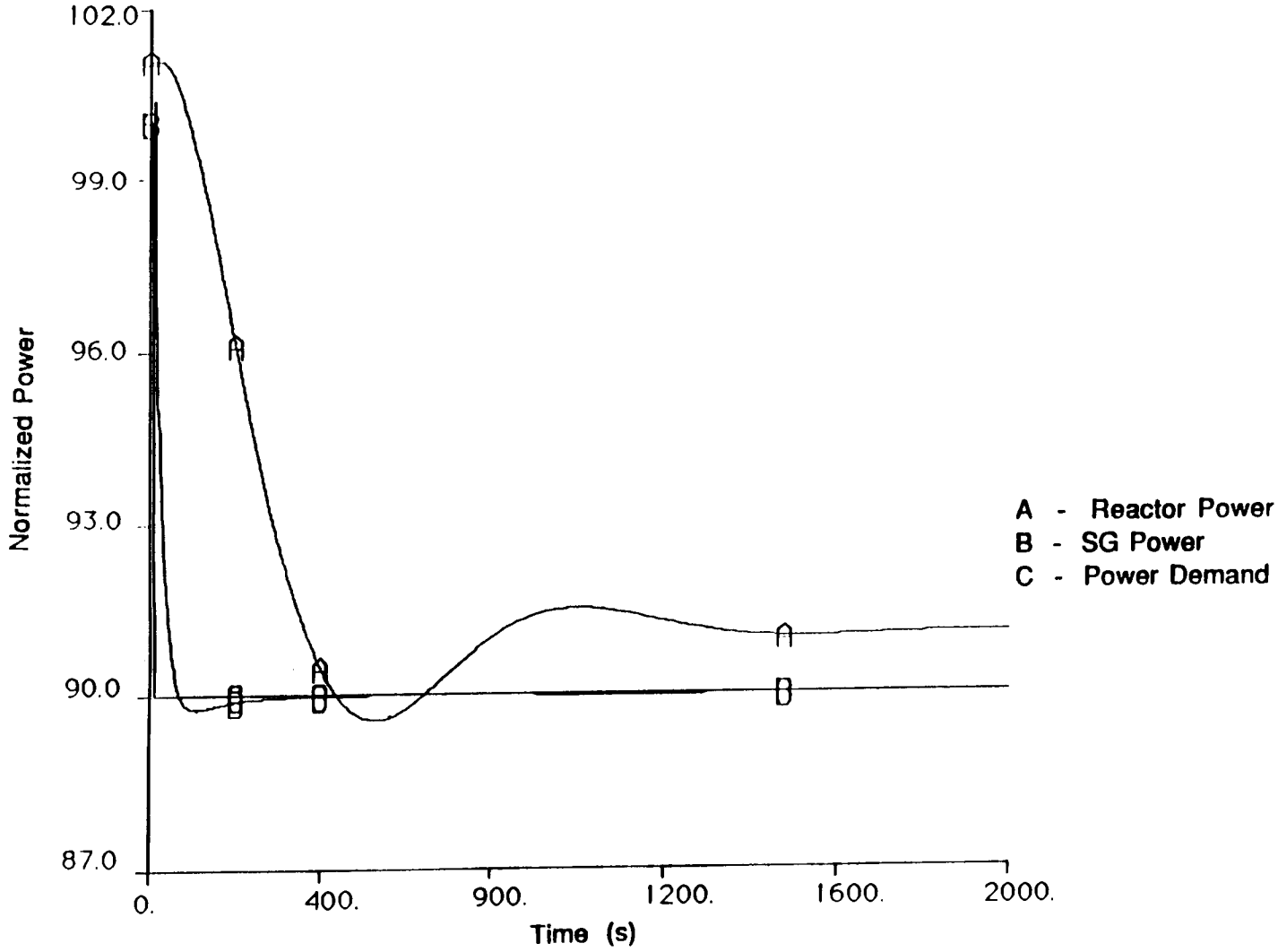

Figure 4.10A 10% Step in Power Demand: Reactor & SG Power.

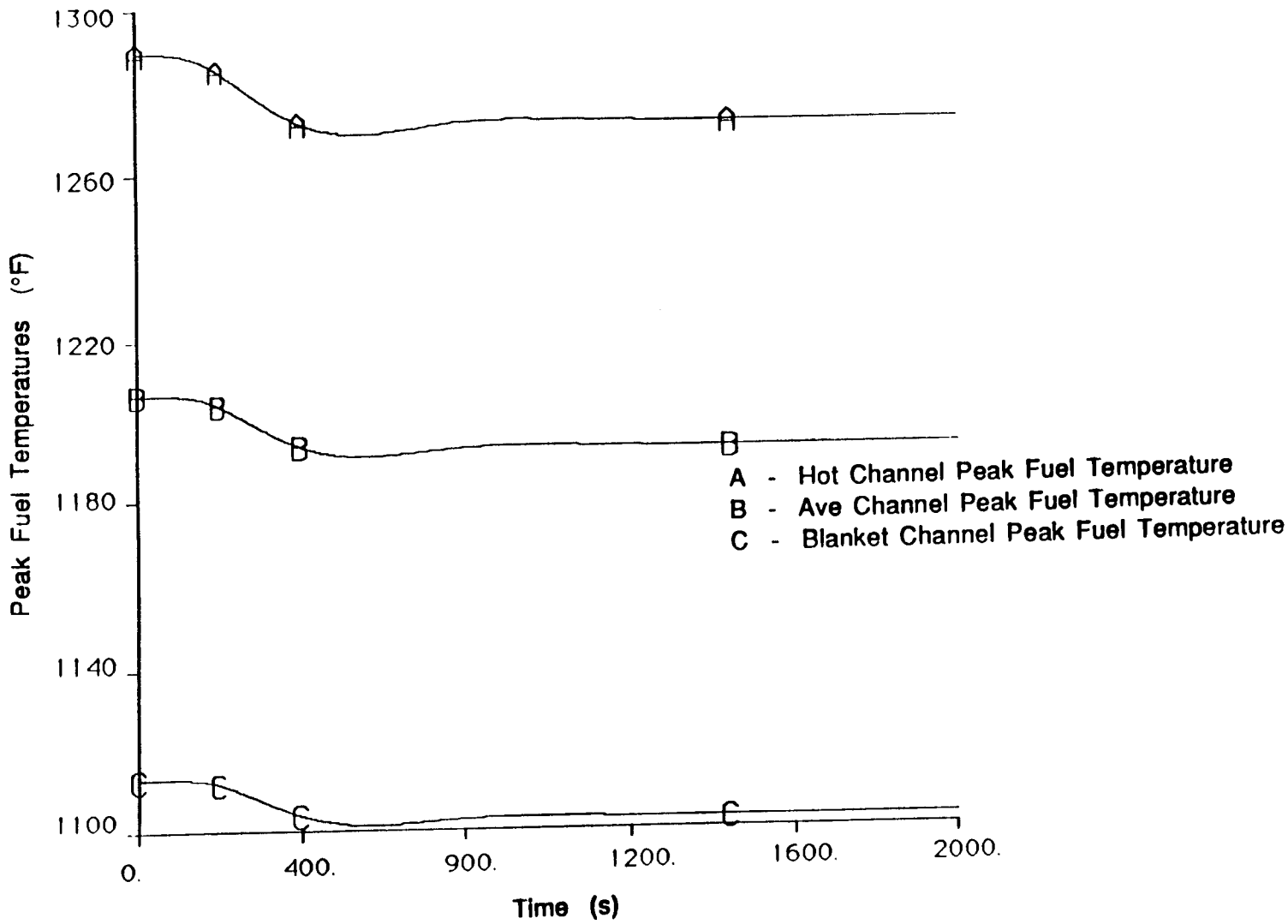

Figure 4.10B 10% Step in Power Demand: Peak Fuel Temperatures.

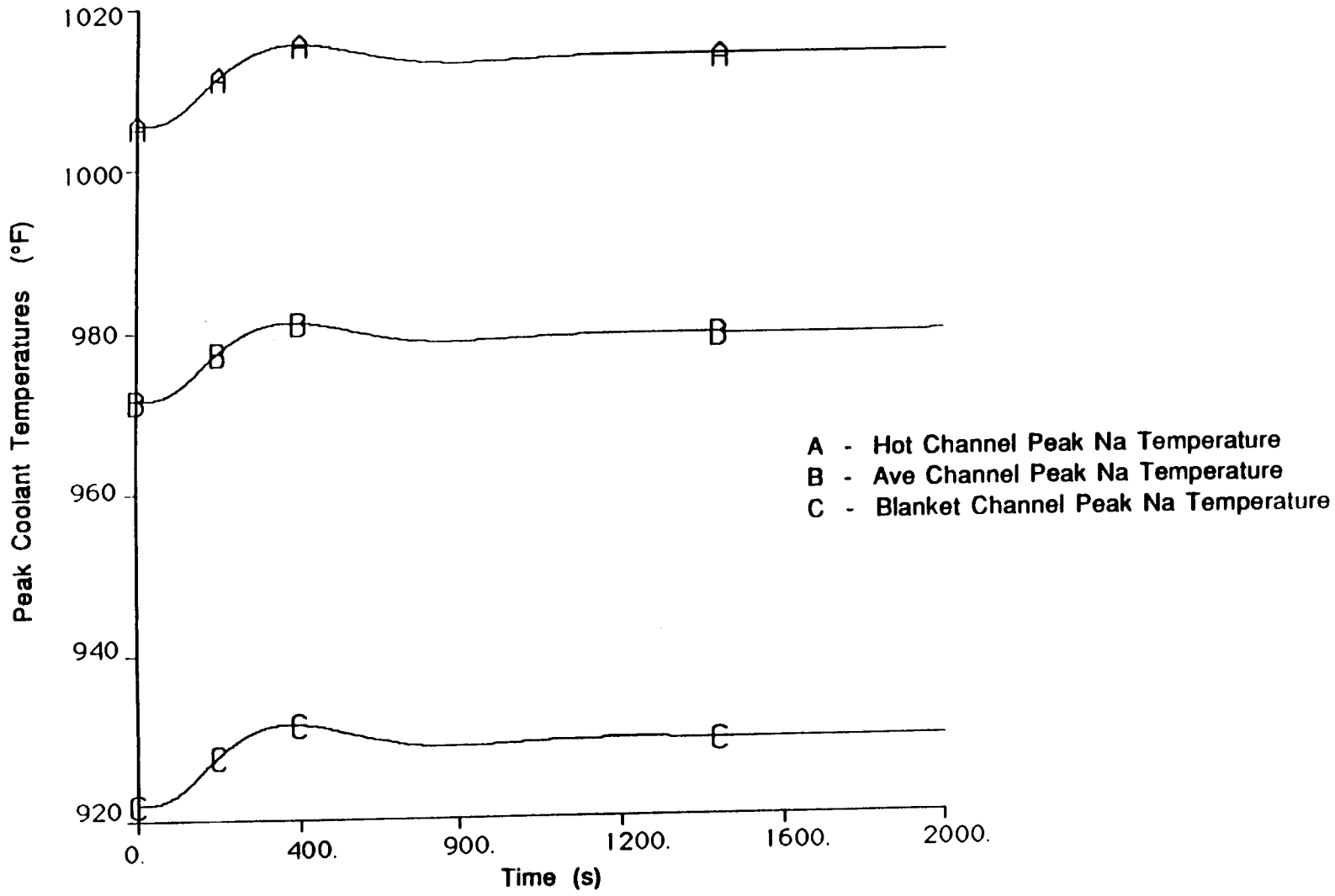

Figure 4.10C 10% Step in Power Demand: Peak Core Coolant Temperatures.

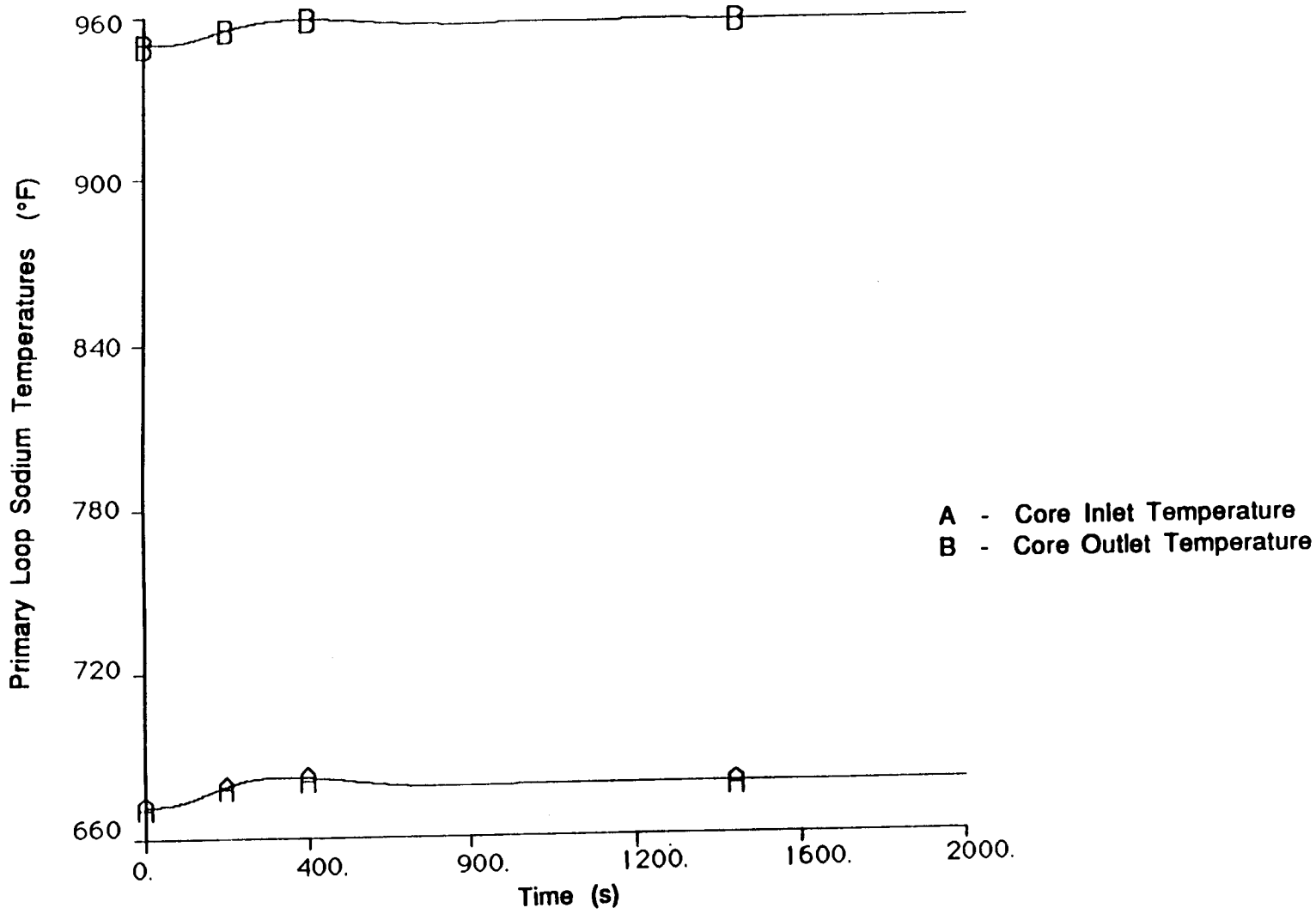

Figure 4.10D 10% Step in Power Demand: Core Inlet & Outlet Temperatures.

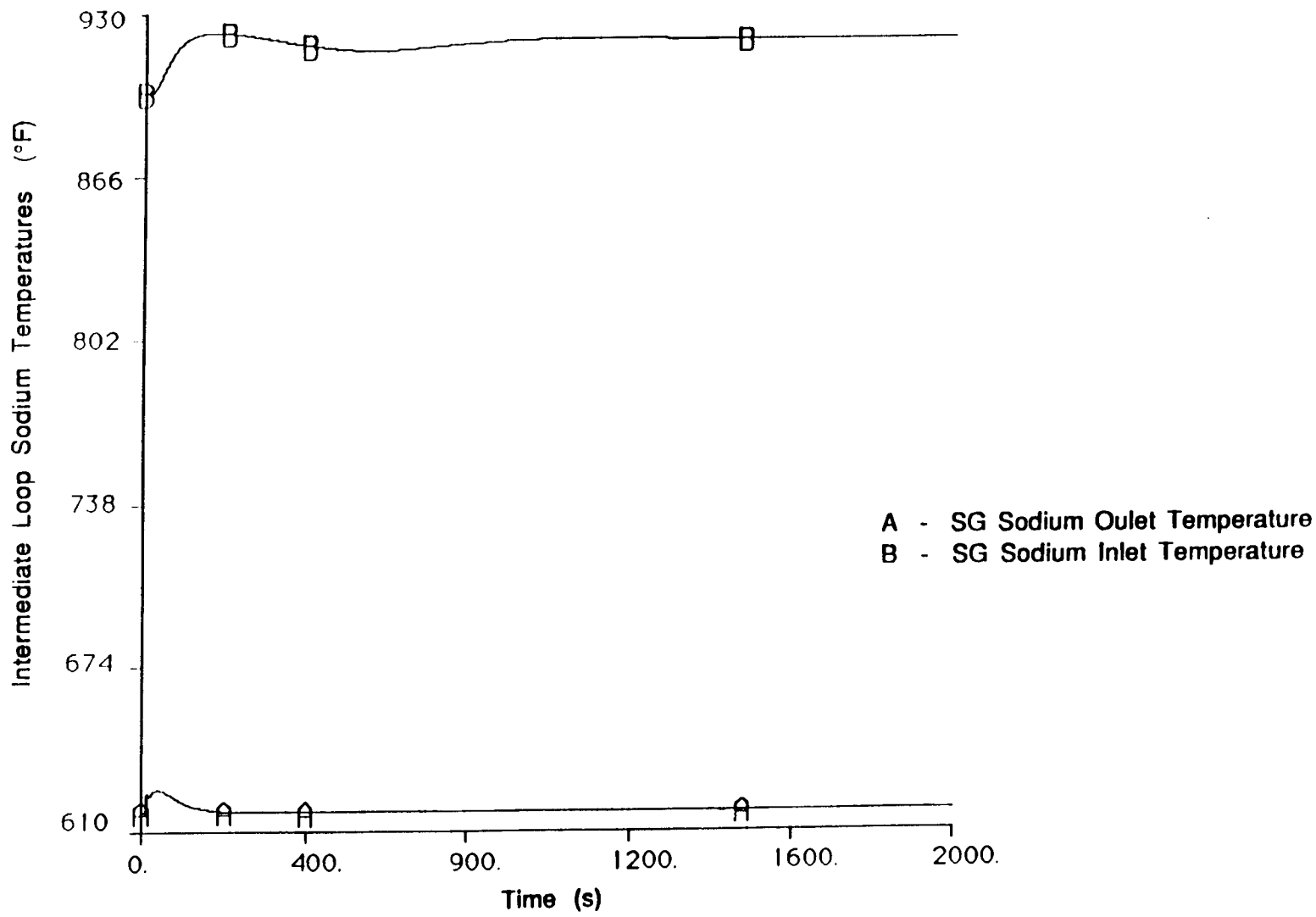

Figure 4.10E 10% Step in Power Demand: SG Inlet & Outlet Temperatures.

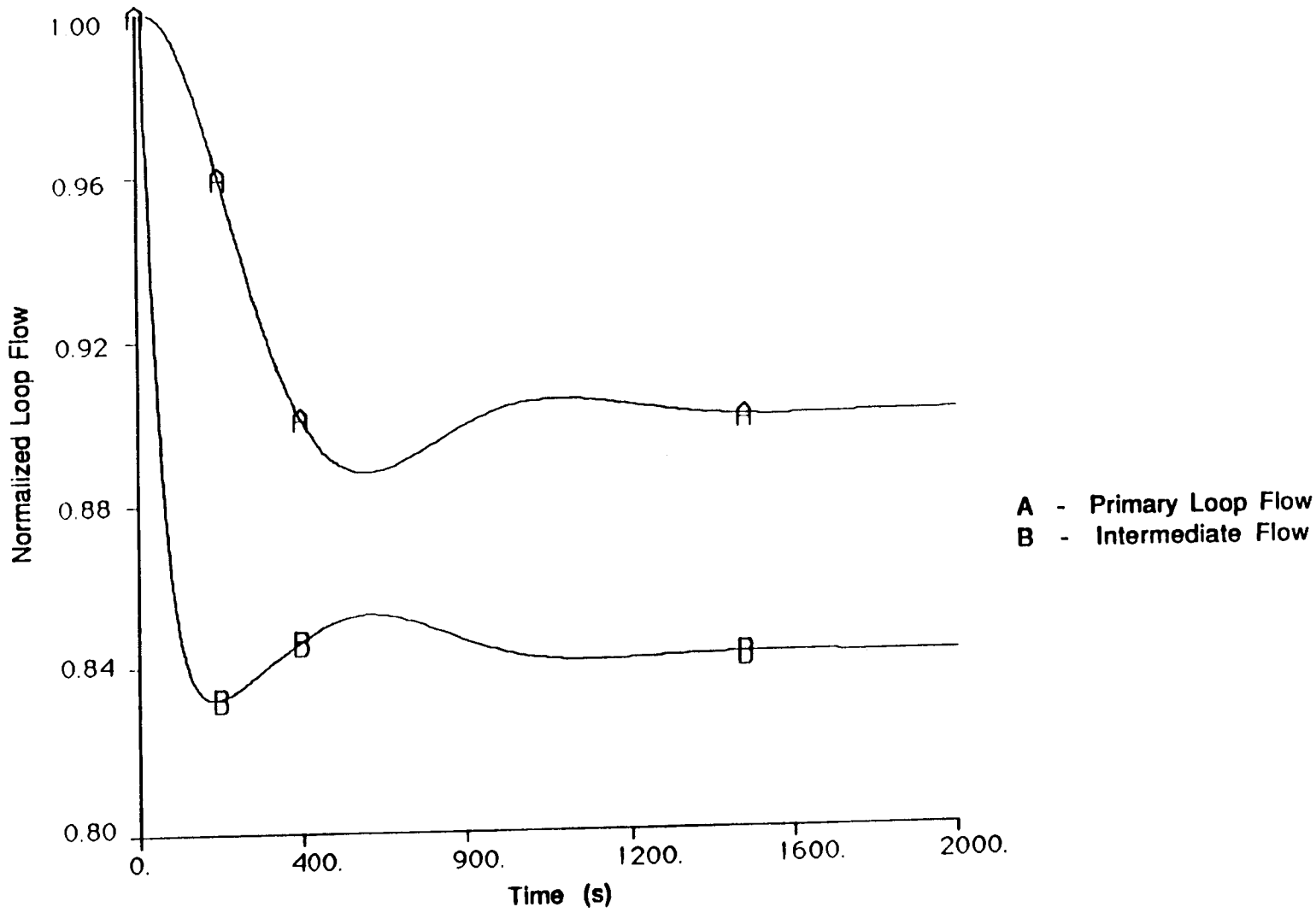

Figure 4.10F 10% Step in Power Demand: Primary & Intermediate Loop Flows.

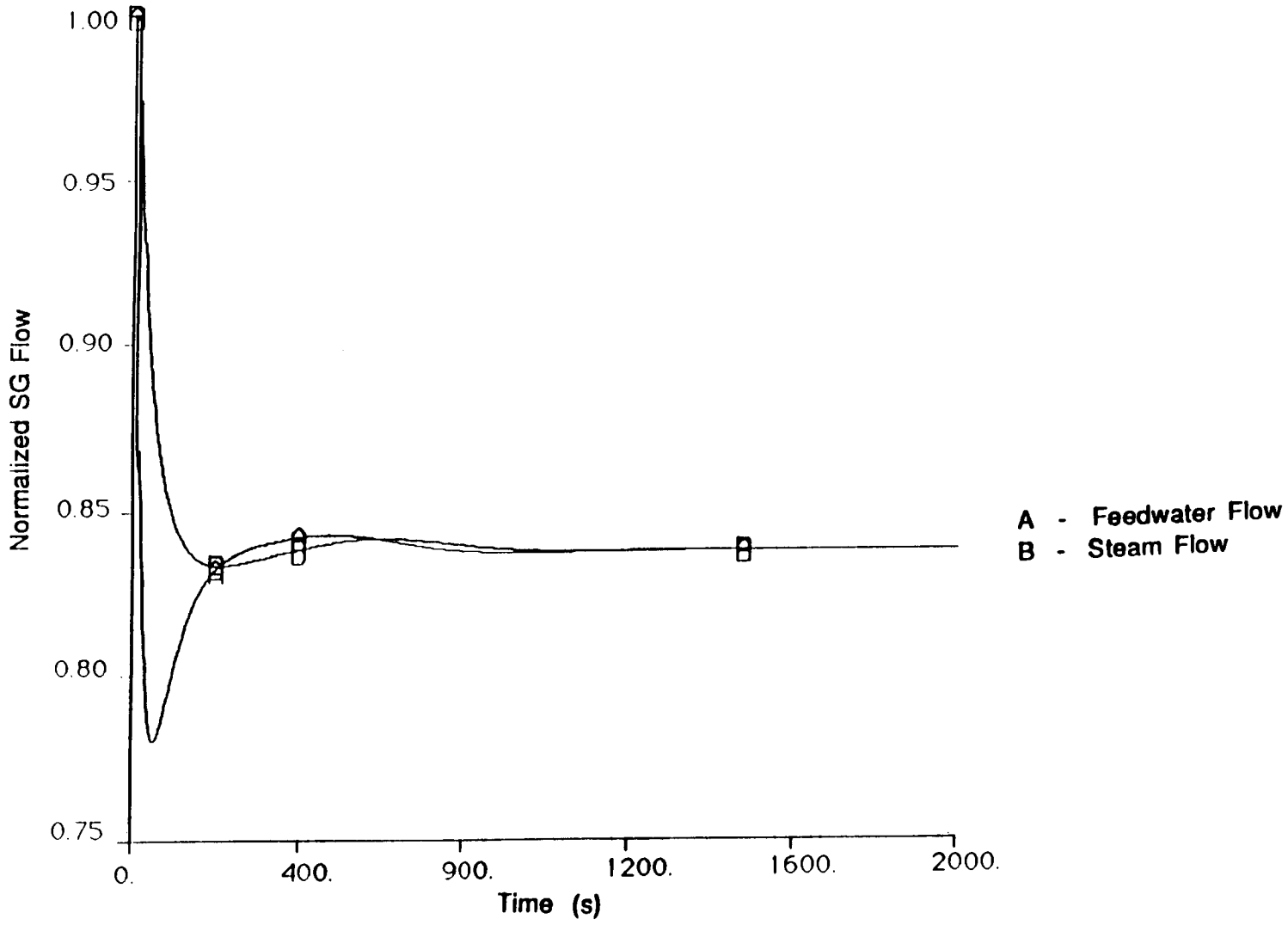

Figure 4.10G 10% Step in Power Demand: Steam & Feedwater Flows.

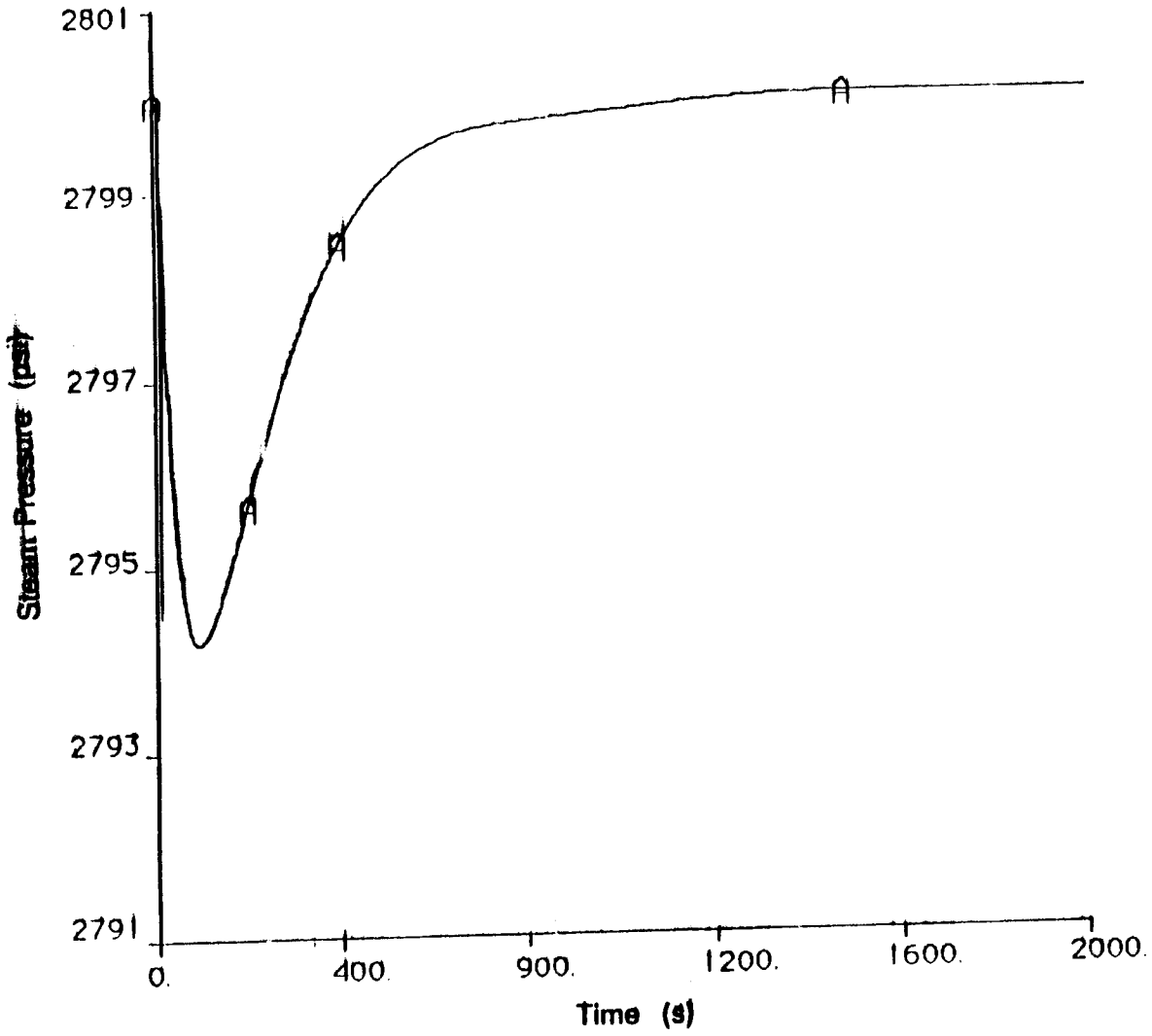

Figure 4.10H 10% Step in Power Demand: Steam Pressure.

5.0 Conclusions

This investigation has evaluated the reactivity feedback mechanisms that lead to the inherent stability of current metal-fueled ALMR designs and used the acquired insight to design and implement an inherent reactor power controller for load following during normal operating conditions. The frequency response of the closed-loop MMS-SAFR model and the time transient test of the inherent reactor power controller have shown the controller to be able to respond to load changes in a rapid yet stable manner. The combined Bode analysis of the response of various system variables to potential controllables and the root locus analysis of the dominant poles of the observable/controllable transfer functions enabled a systematic determination of a "best" set of controller gains. The resulting load following control design strikes a balance between responsiveness and stability.

Inherent power control, as defined in this study, allows neutron power to respond to changes in heat removal through reactivity feedback, as opposed to direct control by rod action. The investigation of the dynamic behavior of the individual reactivity feedback effects demonstrates the prompt, inherently stable, overall reactivity effect following a change in the thermal condition of the core. The reactivity effects of core coolant temperature and fuel temperature provide the net prompt response that permits inherent reactor power control. During a flow reduction transient, the delayed effect of system temperature cooling, given no control action in the balance of plant, results in a power recovery of as much as half the initial reactor power drop, thus counteracting to some degree the prompt inherent feedback response. This effect can be limited by controlling temperatures in the primary and intermediate loops to regulate the long term inherent reactivity behavior. These insights into the natural tendency of the reactor system to seek equilibrium among the reactivity effects facilitate the design of a control system that enhances inherent stability by controlling coolant temperatures via sodium flow variations.

The classical control design developed in this study uses feedwater flow to control steam generator power so that it follows load demand. This control scheme allows for a close coupling between load demand and power delivery to the turbine. Thus, large turbine/generator mismatches are less likely than for a scheme that tries to match reactor power directly to load. The reactor power is inherently controlled by the temperature effects that filter through the intermediate and primary loops. As a result, reactor power lags behind steam generator power by around 200 seconds. The primary flow controller maintains a constant ΔT across the core as the reactor power changes to inherently follow the heat removal change. As indicated in the reactivity feedback effects investigation, controlling the temperature change at the

core inlet reduces the long term recovery effect that the open-loop response showed. The intermediate loop controller maintains a constant sink temperature at the sodium outlet of the steam generator. The selection of the primary and intermediate controllers enhances the inherent reactivity effects and reduces the thermal stresses placed on reactor system components during load change maneuvers.

The study of inherent reactor power control shows that the delayed response of the reactor to steam generator load changes places a stability limit on the reactor load following response. Attempting to speed the response of the system to control action by increasing gains for all controllers leads to less stable behavior. The response of the reactor power to changes caused by controlling steam generator power can only occur as fast as the temperature effects can propagate through the system. The root locus study demonstrated the effect of each controller's gain on the stability of particular system eigenvalues. From this analysis, the performance of the controlled system was evaluated by adjusting gains to determine the proper set that gives the desirable response in a stable fashion.

The 10% step reduction in load demand transient provides an indication of the ability of the inherent reactor power control scheme to meet normal load following events. The design requirements for SAFR specify meeting normal load demand changes by changing power at a rate of 3% per minute within the range of 40% to 100% power. The time transient showed that this control design can better this rate for steam generator power and is only slightly less than this rate (based on rise time) for reactor power. Again, reactor power lags behind the steam generator power but this is a consequence of using a passive scheme for controlling reactor power. The reactivity effects study demonstrated the possibility of using primary flow variations to change reactor power more quickly. It may be feasible to accomplish such control using a feed-forward control scheme for the primary flow controller. However, it is a difficult proposition to control power on two ends of the plant and balance the delayed effects of actions by each controller on the process dynamics at the other end. A multivariate, optimal control design based on this philosophy may achieve faster reactor load following and is recommended for future analysis.

This inherent reactor power control design demonstrates the ability to meet normal load demands without causing large temperature swings in the core. The reactor mixed mean outlet temperature rose a moderate amount in response to a 10% power change and, assuming the temperature rise is linear over the normal operating range, should not exceed 1050°F for a 60% power change. The hot pool temperature for the 10% step underwent a maximum rise of 9°F while the steady state value achieved was 6°F higher than the pre-transient hot pool temperature. The full

range of control for this design can be tested in future research after specifying temperature limits for acceptability and rates of temperature change to evaluate thermal stress on the various cooling system components. The power range for inherent load following control can be determined through time response analysis and the effect of reduced flow conditions on system response time may be evaluated through further frequency analysis. No attempt was made in this study to determine the controller response to more severe duty cycle events that are beyond the range of normal load following transients. It was assumed that the plant protection system or some supervisory plant control system would use control rods to respond to such events. Given the lag between reactor power and balance of plant changes, such action would be necessary to achieve faster response or to limit the temperature swings that might result from more extreme events.

The control design presented takes advantage of the variable speed pumps available in the SAFR system configuration. However, the concept of using the inherent reactivity feedback effects to control neutron power may also be applied to other metal-fueled ALMR designs. Even without flow adjustments to drive the inherent power response for load following, the behavior of reactor power given balance of plant maneuvers should allow some degree of passive control over the 40% to 100% power normal operating range, although there will likely be greater variation in system temperatures than determined in this study for this design. It is recommended that studies be performed on the EBR-II and PRISM LMR designs to determine if similar schemes can be devised that allow the inherent neutron power behavior of metal-fueled reactors to be used to reduce the dependence on control rod insertions for power control or to act as a supplimental power control. Therefore, it may be possible to decrease the required rod worth for the plant control system or define operating regimes where the control rod withdrawal may be locked out. As a result, the potential of a transient overpower without scram accident may be lessened.

Future investigations into inherent reactor power control can determine the sensitivity of the system response to changes in material and nuclear properties, core configuration, and degraded conditions to determine the potential enhancements of the feedback response that can be obtained through altered core design and to ascertain the possible degradation in response due to aging and core burnup effects. Through such work, it may be possible to tune this controller, or similar controllers for other designs, for optimum response at different power levels under different plant conditions. Accounting for the effects of aging and core burnup should allow a more detailed evaluation of the range to which inherent power control can be emphasized and a determination of the rod worth requirements for control over all conditions. In effect, as more information on the dynamic system

is obtained, it will be more likely that the controller performance can be maintained under a variety of conditions. In addition, such information could be used for core design changes to enhance the favorable reactivity feedback effects to yield even more responsive inherent reactor power control.

The inherent reactor power control design for load following in SAFR developed at ORNL represents a starting point that demonstrates the use of the inherent reactivity feedback for passively controlling reactor power in metal-fueled ALMRs. Modern multi-input, multi-output methods, such as linear-quadratic-Gaussian, loop-transfer-recovery (LQG/LTR) and pole placement, could be used to optimize its performance. However, in spite of the lag between steam-side control and reactor power response, it appears the inherent reactor power controller can meet normal load following demands in a stable, responsive manner without causing undue thermal stress within the system.

REFERENCES

1. Rockwell International, "SAFR Sodium Advanced Fast Reactor System Definition Manual", Rockwell International Report 1495DM000001, Rev. C (June 1985).

2. "PRISM Summary Plant Description", W. Kwant,ed., General Electric Report GEFR-00758 (Sept 1985).

3. W. K. Lehto, et al, "Safety Analysis for the Loss-of-Flow and Loss-of-Heat-Sink without Scram Tests in EBR-II", Nuclear Engr. and Design 101 (1987), North Holland-Amsterdam, pp. 35-44.

4. D. Mohr, et al, "Loss-of-Primary-Flow-Without-Scram Tests: Pretest Predictions and Preliminary Results", Nuclear Engr. and Design 101 (1987), North Holland-Amsterdam, pp. 45-56.

5. E. E. Feldman, et al, "EBR-II Unprotected Loss-of-Heat-Sink Predictions and Preliminary Test Results", Nuclear Engr. and Design 101 (1987), North Holland-Amsterdam, pp. 57-66.

6. H. P. Planchon, et al, "EBR-II Unprotected Loss-of-Heat-Sink Predictions and Preliminary Test Results", Nuclear Engr. and Design 101 (1987), North Holland-Amsterdam, pp. 75-90.

7. Private communication, T. Y. C. Wei, ANL (Aug 1988).

8. F. E. Dunn, et al., The SASSYS-1 LMR Systems Analysis Code, ANL/RAS 84-14, Revision 1, March 1987.

9. "Sodium Advanced Fast Reactor (SAFR) Plant Transient Analysis", Rockwell International Report 149ER000002, Rev. A (Aug 1986).

10. Y. I. Chang, J. F. Marchaterre, R. H. Sevy, "The Integral Fast Reactor Concept", Trans. Am. Nucl. Soc.,47, 293, (1984).

11. T. L. Wilson and R. T. Wood, DOE Letter Report, "Liquid Metal Reactor Modeling, Full Plant Models - (Conversion of SASSYS to MMS Format)", August 31, 1988.

12. ACSL - Advanced Continuous Simulation Language, Reference Manual, Mitchell and Gauthier Associates, Concord, MA, Forth Edition, 1986.

13. W. W. Shor, ed., Modular Modeling System (MMS), Volumes 1-5, EPRI CS/NP-3016, April 1987.

14. Private communication, J. E. Cahalan, ANL (June 1988).

15. Matrix$_x$ User's Guide, Integrated Systems Inc., Palo Alto, CA, Version 5.0, October 1985.

16. J. E. Cahalan, R. H. Sevy, and S. F. Su, "Accommodation of Unprotected Accidents by Inherent Safety Design Features in Metallic and Oxide-Fueled LMFBRs", Proc. of Intl. Topical Meeting on Fast Reactor Safety ,Vol. 2, Knoxville, April 21-25, 1985, pp. 29-33.

17. J. E. Cahalan, et al, "Preliminary Safety Assessment of the Integral Fast Reactor Concept", Argonne National Laboratory Report, ANL-IFR-3, (Jan 1985).

18. J. T. Madell, "Analysis of 'Inherently-Safe' Features for Unscrammed Loss-of-Flow Events in LMFBRs", Fauske and Associates, Burr Ridge, IL, FAI/84-57 (Dec 1984).

19. D. Mohr and L. K. Chang, "Perturbations of Reactor Flow and Inlet Temperature for EBR-II Reactivity-feedback Validation", Proc. of Intl. Topical Meeting on Fast Reactor Safety ,Vol. 2, Knoxville, April 21-25, 1985, pp. 617-627.

DISTRIBUTION

U. S. Department of Energy, Washington, DC 20545

1. B. J. Rock, Director, Office of Technology Support Programs, NE-46
2. R. J. Neuhold, Director, Division of Advanced Technology Development, NE-462
3. H. Alter, Division of Advanced Technology Development, NE-462

4-5. DOE Office of Scientific and Technical Information, P. O. Box 62, Oak Ridge, TN 37831

6. G. Santos-Leon, Energy Programs Division, U.S. Department of Energy, Oak Ridge Operations Office, P.O. Box E, Oak Ridge, TN 37831
7. J. I. Sackett, Argonne National Laboratory, 9700 South Cass Avenue, Argonne IL 60439
8. H. P. Planchon, Argonne National Laboratory, 9700 South Cass Avenue, Argonne IL 60439
9. J. E. Cahalon, Argonne National Laboratory, 9700 South Cass Avenue, Argonne IL 60439
10. T. Y. C. Wei, Argonne National Laboratory, 9700 South Cass Avenue, Argonne IL 60439
11. J. Brunings, Rockwell International, Rocketdyne Division, 6633 Canoga Avenue, Canoga Park, CA 91304
12. R. Mucica, Rockwell International, Rocketdyne Division, 6633 Canoga Avenue, Canoga Park, CA 91304
13. E. Moore, Rockwell International, Rocketdyne Division, 6633 Canoga Avenue, Canoga Park, CA 91304
14. D. Carroll, General Electric Company, Nuclear Systems Technology Operation, P.O. Box 530954, San Jose, CA 95153-5354
15. Y. Dayal, General Electric Company, Nuclear Systems Technology Operation, P.O. Box 530954, San Jose, CA 95153-5354
16. W. Wagner, General Electric Company, Nuclear Systems Technology Operation, P.O. Box 530954, San Jose, CA 95153-5354

Oak Ridge National Laboratory, P.O. Box 2008, Oak Ridge, TN 37831-6010

17. J. L. Anderson
18. S. J. Ball
19. C. R. Brittain,
20. N. E. Clapp,

21. B. G. Eads
22. D. N. Fry
23. J. E. Jones Jr.
24. R. A. Kisner
25. G. Murphy
26. P. J. Otaduy
27. J. T. Robinson
28. R. L. Shepard
29-33. J. D. White
34. T. L. Wilson
35. R. T. Wood
36-37. Laboratory Records (2)
38. Laboratory Records - RC
39. I&C Division Publications Office

40. B. R. Upadhyaya, University of Tennessee, Department of Nuclear Engineering, 315 Pasqua Building, Knoxville, TN 37966
41. R. Perez, University of Tennessee, Department of Nuclear Engineering, 315 Pasqua Building, Knoxville, TN 37966
42. M. Bailey, University of Tennessee Department of Electrical and Computer Engineering, Knoxville, TN 37996-2100